A&A 578, A87 (2015)
DOI: 10.1051/0004-6361/201424281

Astronomy & Astrophysics

Reconstructing the star formation history of the Milky Way disc(s) from chemical abundances

O. Snaith[1,2], M. Haywood[1], P. Di Matteo[1], M. D. Lehnert[3], F. Combes[4], D. Katz[1], and A. Gómez[1]

[1] GEPI, Observatoire de Paris, CNRS, Université Paris Diderot, 5 place Jules Janssen, 92190 Meudon, France
[2] Department of Physics & Astronomy, University of Alabama, Tuscaloosa, Alabama, USA
e-mail: owain.n.snaith@ua.edu
[3] Institut d'Astrophysique de Paris, UMR 7095, CNRS, Université Pierre et Marie Curie, 98bis Bd Arago, 75014 Paris, France
[4] LERMA, Observatoire de Paris, CNRS, 61 Av. de l'Observatoire, 75014 Paris, France

Received 26 May 2014 / Accepted 5 November 2014

ABSTRACT

We develop a chemical evolution model to study the star formation history of the Milky Way. Our model assumes that the Milky Way has formed from a closed-box-like system in the inner regions, while the outer parts of the disc have experienced some accretion. Unlike the usual procedure, we do not fix the star formation prescription (e.g. Kennicutt law) to reproduce the chemical abundance trends. Instead, we fit the abundance trends with age to recover the star formation history of the Galaxy. Our method enables us to recover the star formation history of the Milky Way in the first Gyrs with unprecedented accuracy in the inner ($R < 7-8$ kpc) and outer ($R > 9-10$ kpc) discs, as sampled in the solar vicinity. We show that half the stellar mass formed during the thick-disc phase in the inner galaxy during the first 4−5 Gyr. This phase was followed by a significant dip in star formation activity (at 8−9 Gyr) and a period of roughly constant lower-level star formation for the remaining 8 Gyr. The thick-disc phase has produced as many metals in 4 Gyr as the thin-disc phase in the remaining 8 Gyr. Our results suggest that a closed-box model is able to fit all the available constraints in the inner disc. A closed-box system is qualitatively equivalent to a regime where the accretion rate maintains a high gas fraction in the inner disc at high redshift. In these conditions the SFR is mainly governed by the high turbulence of the interstellar medium. By $z \sim 1$ it is possible that most of the accretion takes place in the outer disc, while the star formation activity in the inner disc is mostly sustained by the gas that is not consumed during the thick-disc phase and the continuous ejecta from earlier generations of stars. The outer disc follows a star formation history very similar to that of the inner disc, although initiated at $z \sim 2$, about 2 Gyr before the onset of the thin-disc formation in the inner disc.

Key words. Galaxy: disk – Galaxy: evolution – Galaxy: formation – Galaxy: structure – solar neighborhood

1. Introduction

The basis of Galactic archaeology is the assumption that the signatures of the formation history of the Milky Way are encoded into the distribution and properties of stellar populations. Thus, the history of star formation is assumed to be impressed into the chemical properties of stars. Translating the observed metallicity of stellar populations into a star formation history (SFH) is not trivial, however, and is an ongoing process because we are constantly improving observations and developing better models.

The overwhelming majority of the current chemical evolution models are based on the observation that the disc in the solar neighbourhood contains far too few metal-poor stars – here, "metal-poor" means about 1/3 of the solar metallicity (e.g. Binney & Merrifield 1998; Tinsley 1974; Schmidt 1963; Pagel & Tautvaisiene 1997; Pagel & Patchett 1975; van den Bergh 1962) – to have formed from a very gas-rich, low-metallicity, interstellar medium (ISM) at early times. This is the so-called G-dwarf problem. To overcome this lack of intermediate-metallicity stars, most studies have endorsed the idea that the gas must have been conveyed onto the disc on a relatively long time-scale, maintaining a small gas reservoir, a limited dilution and, consequently, a rapid rise of the metallicity in the ISM before many stars formed.

This approach constitutes the basis of current Galactic chemical evolution (GCE) codes (e.g. Chiosi 1980; Chiappini et al. 1997; Fenner et al. 2002), which assume an open-box model, where gas falls into the galaxy over time. The density of the gas is then used to calculate the star formation rate (SFR) according to a Schmidt-Kennicutt relation (Kennicutt 1998). The rate of infall is then tuned to recover the surface density of the Milky Way, the current gas fraction, the current SFR, etc. At this point, the chemical evolution of the system is examined, usually against a metallicity-[α/Fe] distribution. The particular form of the gas inflow(s) (or outflow(s)) can then be varied to improve the fit to the data. Thus, we have dual-infall models (Chiappini et al. 1997; Fenner et al. 2002), three-infall models (Micali et al. 2013), two inflows and an outflow (Brusadin et al. 2013), etc. These models also often require tuning in terms of the star formation (e.g. Chiappini et al. 1997 use twice the value of their star formation tuning parameter during the halo-thick-disc phase than in the thin-disc phase).

However, in the past few years, a number of new results have forced us to revise our current picture of the Galaxy and of the link between its stellar populations and their mass budget. There is now evidence for a direct chemical and kinematic continuity between the thick and thin discs, both on large (Bovy et al. 2012) and local (Haywood et al. 2013) scales. It would be extremely difficult to imagine that such a large structure, with similarities to the halo and the bulge, could have been accreted (Abadi et al. 2003). Moreover, recently measured structural parameters of the thick disc by Bensby et al. (2011) and Bovy et al. (2012) indicate that this population is massive (see the discussion below and

Fuhrmann et al. 2012). Hence, there is now increasing evidence that a significant amount of low-metallicity stars (in the sense defined above, and which correspond to the thick-disc metallicity) exist in the Galaxy, although most must be confined at Galactic radii smaller than the solar circle (in the inner disc).

The most intense phase of star formation in the Universe occurred at redshifts between 2 and 3 (Hopkins & Beacom 2006; Madau et al. 1996, 1998; Lilly et al. 1996; Madau & Dickinson 2014). The thick disc represents the only stellar population in the Galaxy that corresponds to this star formation phase, because the classical spheroid, if present, contributes only mildly to the total mass (Carney et al. 1990; Shen et al. 2010; Kunder et al. 2012; Di Matteo et al. 2014). But, the thick disc is either absent from most chemical evolution models or its role is severely underestimated (however, see Gilmore & Wyse 1986). The reason for this is that models are fitted to the solar neighbourhood, where the thick disc represents only about 10% of the local stellar density (Jurić et al. 2008). However, the population fractions measured in the solar vicinity are not representative of the entire Galaxy (see Sects. 3.2 and 7). While the use of population fractions in the solar neighbourhood may, therefore, be misleading in efforts to recover the SFH of the early stages of the Galaxy and the corresponding stellar mass formed at those times, chemical abundances are not: indeed, thick-disc stars found at the solar vicinity were born at very different radii (e.g. Reddy et al. 2006), making them representative of the whole thick-disc population, see Sect. 3.2. Their chemical enrichment patterns, as found in the solar neighbourhood, are the imprints left by a formation phase that involved the entire disc.

The present study is, therefore, an attempt to re-examine the question of the chemical evolution of the Galaxy from the very beginning and from its simplest form in light of the most recent results obtained in the field of Galactic stellar populations. In an effort to reduce the number of assumptions to a minimum, we model the inner disc system using a closed-box model, providing physical arguments to show that this is more than an academic exercise and that it must be considered as a good first-order representation of the evolution of the Milky Way disc. The outer disc system is modelled as essentially the same sort of closed-box system, but with a single infall event to reduce the metallicity. In Snaith et al. (2014), we described our first results on the derivation of the SFH of the inner Galactic disc(s). In the present study, we provide a full description of our model, an in-depth assessment of the various sources of errors in the derivation of the SFH, and a derivation of the SFH of the outer disc. By means of the chemical data and their evolution with time, which was recently discussed in Haywood et al. (2013), we show that the thick-disc formation phase accounts for about half of the stellar material present in the Milky Way. This indicates that a revision of the mass budget in the Galactic thin and thick discs is necessary, as well as of the amount of star formation required in the early phase of the Galactic evolution and of the gas reservoir that must have been available at high redshifts in the Galaxy.

We first present the model (Sect. 2). We then outline the key points of the data and our understanding of recent observational results of importance to our study in Sect. 3. We explore, in a general way, how changing the SFH affects the chemical evolution history of the ISM, with regard to the silicon and iron abundances (Sect. 4). We determine the SFH that best fits the observational silicon data in Sect. 5, examine how the results of the model are affected by our choice of parameters and dataset (and chosen elements) in Sect. 6. Finally, we discuss our results in Sect. 7.

2. Model

2.1. Modelling philosophy

Our basic approach was to develop a simple model, using the fewest possible assumptions. We discuss below why these assumptions are not unrealistic.

A GCE model is a very simple model of the chemical history of a galaxy and uses a set of simple recipes to follow galaxy evolution. A strength of this approach is that the effect of different scenarios can be very quickly studied, while more elaborate models and simulations can make it harder to distinguish the effects of different processes.

We therefore developed a model where (1) the ISM is considered to be always well mixed; (2) the initial mass function (IMF) is time independent; (3) the initial metallicity of the ISM is negligible; (4) the system is closed in the inner disc and (5) the outer disc experiences a single accretion event at a look-back time of 10 Gyr. This accretion event is a simple dilution of the in-situ gas by gas with primordial abundance and is required to match observations, see Haywood et al. (2013).

We did not assume instantaneous recycling and took into account the stellar lifetimes. The impact of this depends on the time step of the model. If the time step is large, then all the gas and metals from core collapse supernovae (SNII) are returned at once anyway.

Are these assumptions realistic?

1. We know from several indicators (Cartledge et al. 2006) that the ISM is homogeneous on scales of a few hundred parsecs. There are indications that it has remained so in the past, with evidence from pre-solar grains formed during the thin-disc formation (4.6 Gyr ago, Nittler 2005). Similar homogeneity can be inferred for the thick disc from the tight age-metallicity and age-α abundance ratios that have been measured by Haywood et al. (2013). As explained in Haywood et al. (2013), the apparent dispersion in the age-metallicity relation of thin-disc stars in the solar vicinity (age < 8 Gyr) can be explained if the Sun lies at the interface between the inner and outer discs. It is, therefore, polluted by stars from both discs through the epicyclic radial oscillation of stars. It remains, however, that the assumption of an homogeneous ISM is a reasonable one.
2. Even the most sophisticated chemical evolution models consider the IMF to be time-independent, and it is only for the very first generation of stars that any convincing evidence has been proposed that the IMF might be different (top-heavy) (Yamada et al. 2013).
3. The initial metallicity of the thick disc is at least two orders of magnitudes below solar ([Fe/H] < -2 dex, Morrison et al. 1990; Reddy et al. 2006; Kordopatis et al. 2013), which, in practice, means that essentially all Galactic chemical enrichment – and therefore most of the metallicity distribution – is the result of the (thin+thick) disc formation phase. Our assumption that the model starts with zero initial metallicity can be considered a good first-order approximation.
4. Can the inner disc system be considered closed? In this form the question looks largely academic: we know the system was most probably "open" at an epoch when interactions with the environment must have been intense. This question can, however, be reformulated as follows: how much gas was available for rapid consumption in the first few Gyr? The time-scale of the gas accretion is unknown. What is observed, however, is that discs at redshift ~2 are rich in gas (Tacconi et al. 2010). In the present study, we assume that

the closed-box model either approximates a situation where most of the accretion in the inner disc ($R < 10$ kpc) has occurred early in the evolution of the Galaxy, or a situation where the gas accretion maintains a gas fraction sufficiently high that the disc evolution is not directly dependent on the accretion history. That copious amount of gas must have been available in the first few Gyr of the Galaxy is therefore in accordance with the observation of discs at high redshift, and with the recent estimate of the mass of the thick disc in the Milky Way (see comment in Haywood et al. 2013; Haywood 2014; Snaith et al. 2014). This is at variance with standard chemical evolution modelling, where gas accretion is scarce.

With these assumptions we explore the characteristics of the chemical tracks of stars in the solar neighbourhood, and their evolution with time (see Adibekyan et al. 2012; Haywood et al. 2013, and Sect. 3.2). This is done to recover the SFH that best fits the data. We identify the best SFH by constraining it with the chemical characteristics of stars in the solar vicinity, and are able to quantify the chemical enrichment track that a given SFH produces. To this end, we have developed a chemical evolution code and describe it in Sects. 2.2 and 2.3. The code can be broken up into two sections. The first (part A) reads the chemical yields and converts them into a chemical evolution for a simple stellar population (SSP) of a given initial metallicity, Z. The second (part B) uses these tracks and traces the chemical enrichment of the ISM due to a given SFH.

In a departure from standard chemical evolution codes, we do not assume any specific form of the Kennicutt-Schmidt (Schmidt 1959; Kennicutt 1998) law to link the gas and SFR densities. The two quantities are decoupled. This means that at any given time, part of the gas in the system is used to make stars, while the remaining part can be seen as the gas reservoir for subsequent star formation. Because the SFR is the quantity we wish to constrain, this approach is justified and will allow us to avoid developing any hypothesis on the precise form of the specific Schmidt law (Schmidt 1959).

When we call the inner disc "closed" we mean that the gas present at the beginning is eligible to form stars and at the same time acts as a reservoir of primordial gas into which the metals are injected. We do not specify whether this gas is cold gas in the disc of the galaxy (the cold ISM), warm gas in the Galactic corona, or hot gas in the halo. This means that the closed box system consists of gas that can cool to form stars and can act to dilute the metals ejected by stars.

In the following (Sects. 2.2 and 2.3), we describe the key features of our chemical evolution code.

2.2. Making chemical evolution tracks (Part A)

This first part of the code generates the chemical evolution tracks. The tracks provide the normalised mass (if the initial stellar population has a mass of 1) of metals or gas released from a stellar population of given metallicity after a given amount of time. We use a grid of nine metallicity values ranging from 0 to $Z_\odot$, and calculate the cumulative amount of metals released over 14 Gyr. We assume that metals are produced from SNII, SNIa, and asymptotic giant branch (AGB) stars. The time step increases exponentially with the age of the population. This is because most metals are released within the first few Gyr, and so we must trace the early release with greater resolution.

The steps involved in generating these tracks are as follows:

1. Choose an IMF (i.e. Kroupa 2001).
2. Choose the yields for SNII, AGB, and SNIa.
3. Derive stellar life times.
4. For each Z in the grid, calculate the mass fraction of stars that are SNII and AGB at a given time t.
5. Multiply step 4 by the yields.
6. Define the functional form of the SNIa time delay, multiply by the SNIa yields.
7. Cumulatively sum the yields with increasing time.

This part of the code allows us to calculate the amount of gas returned, the mass of the various species of metals, the number of SNII or SNIa at a given time, etc. for a stellar population for a given initial metallicity.

We used the yields reported by Nomoto et al. (2006) for SNII[1]. This was required if the [Si/Fe] is to have a high enough maximum value at the beginning of the model run. At the lower end of the SNII mass distribution, we assumed that the minimum mass of SNII stars is 8 solar masses (e.g. Few et al. 2012; Kawata & Gibson 2003, etc.), unfortunately the SNII yields only reach down to approximately 12 solar masses. We therefore extrapolated down to 8 by scaling proportionally to the mass. In other words, we took the yield of stars at 12 solar masses and multiplied them by two thirds to derive the expected yield at 8 solar masses (Few et al. 2012). We also extrapolated the Karakas (2010) AGB yields down to 0.1 solar masses in the same way. By scaling the lower end of the iron yields by the stellar mass, we introduced an uncertainty of ~15%, which is a relatively small difference.

For the SNII yields, the lowest metallicity in the theoretical yield tables is $Z = 0$, meaning a pristine star, while the highest is $Z = 1\ Z_\odot$ or solar metallicity. Where the metallicity of the star exceeds $1\ Z_\odot$, we assumed that the stellar yield is the same as if it were still at $1\ Z_\odot$. Similarly, where the derived AGB metallicities lay above or below the metallicities given in the tables, we assumed that any chemical yields were the same as at the extremity of the table.

None of the theoretical yields for SNII we used provided values for stellar masses greater than 40 solar masses. α-elements scale strongly with mass, between 8 and 40 solar masses, while the iron value does not. If we assume that stars with masses greater than 40 solar masses all have yields the same as stars at 40 solar masses (as in Few et al. 2012; Kawata & Gibson 2003), we cannot arrive at a solution for silicon. We therefore only include stars with masses of up to 40 solar masses in our SNII yield tables. The uncertainties in the various yield tables (e.g. Nomoto et al. 2006; Limongi & Chieffi 2002; Woosley & Weaver 1995) mean that this is no worse an assumption than alternative approximations. Ideally, we await yields that extend to 100 solar masses and are greater than solar metallicity to reduce this avenue of uncertainty.

The tables of yields are given according to the mass of the star ejecting those metals. We used the simple analytical fit of Raiteri et al. (1996) to calculate the stellar lifetimes,

$$\log(t_*) = a_0(Z) + a_1(Z)\log M + a_2(Z)\log M^2, \quad (1)$$

where
$a_0(Z) = 10.13 + 0.07547\log Z - 0.008084\log Z^2$
$a_1(Z) = -4.424 + 0.7939\log Z - 0.1187\log Z^2$
$a_2(Z) = 1.2662 + 0.3385\log Z - 0.05417\log Z^2$,
where Z is the metallicity and M is the mass of the star.

[1] In Sect. 6.5 we also used yields derived by Woosley & Weaver (1995). These yields were modified according to Timmes et al. (1995), where the iron yield is reduced by a factor of two.

Equation (1) is valid within the metallicity range of 7×10^{-5} to 3×10^{-2}, therefore, we set them to 3×10^{-2} (7×10^{-5}) for use in this equation, for metallicities greater (lower) than this. We rearranged Eq. (1) to solve for M to determine the mass of stars that end their lives at a given time step.

We also convolved the yield tables with an IMF. We use the Kroupa (2001) IMF in Sects. 4, 5, and most of Sect. 6 (normalised to between 0.1 and 100 solar masses) because it is a simple, basic and commonly used IMF. The particular form of the IMF is

$$\Phi(m) = \begin{cases} 0.332m^{-0.8} & 0.1 < m \leq 0.5 \\ 0.178m^{-1.7} & 0.5 < m \leq 1 \\ 0.178m^{-1.3} & 1 < m \leq 100. \end{cases} \quad (2)$$

A discussion of the particular choices of IMF and yields used in the model is discussed in Sects. 6.3, 6.5, and 6.6.

To combine the yields, stellar lifetimes, and IMF, we use

$$\Gamma(t = now) = \int_{t=0}^{t=now} \frac{\Phi(M(t))}{M(t)} \gamma(M(t)) \mathrm{d}t, \quad (3)$$

where $\Gamma(t)$ is the integrated yield with time, $\Phi(M(t))$ is the IMF of the stars dying at t, and $\gamma(M(t))$ is the stellar yield of the stars dying at t.

Finally, we included the chemical yields of the SNIa from Iwamoto et al. (1999). We used the supernova rate given in Kawata & Gibson (2003), which is based on the paper by Kobayashi et al. (2000). This approach divides the potential SNIa host systems into those that contain a white dwarf and a red giant and those that contain a white dwarf and a main-sequence star. In effect, this delays adding elements from SNIa by 1 to 2 Gyr. Here, we have to assume that a SNIa returns 1.38 solar masses to the ISM, which completely destroys the white dwarf. We also assume that the amount of hydrogen fed back into the ISM is 0.01 solar masses per supernova. The actual contribution of hydrogen from SNIa is negligible compared to the SNII and AGB contributions, so this value is essentially everything that is not metals. In general, however, this value is unimportant for deriving the [Fe/H] value from the model. Several authors have used a minimum metallicity below which SNIa are assumed not to occur (Kobayashi et al. 2000). In general, we neglect this, but discuss the effect it has on our model in Sect. 6.

The form of the SNIa time-delay distribution is still debated, with numerous functional forms available in the literature (e.g. Kobayashi et al. 1998; Greggio 2005; Matteucci et al. 2009). We chose the following form, given in Kawata & Gibson (2003):

$$N_{\mathrm{SNIa}}(t) = f_{\mathrm{p}}(m) \times (g_{\mathrm{h,MS}}(m) + g_{\mathrm{h,RG}}(m)) \quad (4)$$

$$f_{\mathrm{p}}(m) = \int_3^8 \frac{\Phi(M)}{M} \mathrm{d}m \quad (5)$$

$$g_{\mathrm{h,MS}}(m) = b_{\mathrm{MS}} \frac{\int_{\max(1.8,m(t))}^{2.6} \Phi(m)\mathrm{d}m}{\int_{1.8}^{2.9} \Phi(m)\mathrm{d}m} \quad (6)$$

$$g_{\mathrm{h,RG}}(m) = b_{\mathrm{RG}} \frac{\int_{\max(0.9,m(t))}^{1.5} \Phi(m)\mathrm{d}m}{\int_{0.9}^{1.5} \Phi(m)\mathrm{d}m}, \quad (7)$$

where $N_{\mathrm{SNIa}}(t)$ is the number of supernovae with time, $\Phi(m)$ is the IMF, 8 and 3 are the masses of the stars that evolve into white dwarfs, (2.6, 1.8) and (1.5, 0.9) are the mass range of stars that fuel the white dwarf and are either main-sequence stars or red giants. In this single-degenerate model, we neglect the contribution of binary white dwarf pairs. These pairs may provide another path to SNIas. Such a double-degenerate model could provide a drawn-out tail of SNIa with very long time-delay (Greggio 2005). SNIa produce 0.75 solar masses of iron and 0.16 solar masses of silicon. The cumulative number of SNIa ($N_{\mathrm{SNIa}}(< t)$) is shown in Fig. 1.

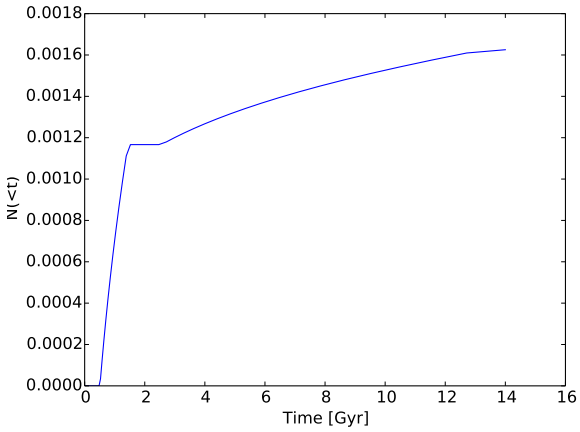

Fig. 1. Time-delay distribution of SNIa for solar metallicity stars. The blue line shows the cumulative number of SNIa expected from an SSP.

At every time, t, since the formation of the stellar population we calculated the cumulative yield of various chemical elements (O, Mg, Si, Fe), the total metallicity (Z), and total gas released since $t = 0$. After defining the yields at a given mass and the relation between mass and stellar lifetime, we produced the cumulative metal release for a given stellar population with a given IMF for a given set of stellar yields.

We summed the amount of metals produced in descending order of mass and plot this against stellar lifetime. This was then used to generate a table that lists how a given stellar population ejects metals with time.

2.3. Calculating the GCE (Part B)

Part B then uses the tables created by the above approach and calculates the chemical evolution of the system that a given SFH produces.

The GCE code models the galaxy and follows the mass of metals and gas present in the ISM with time. Of particular interest to this paper is the mass of α-elements (e.g. Si, Mg, O), Fe, H, and total gas present. From these data we can follow the evolution of the metallicity, gas fraction, abundance ratios, etc. at each time step.

At $t = 0$ the system contains pristine gas of mass 1, composed of 0.75 hydrogen and 0.25 helium. We normalised the SFH such that the integral of the SFR over 14 Gyr is equal to 1. Because mass is released back into the gas phase due to supernovae and stellar winds, the total stellar mass at the end of the evolution is never itself equal to 1, but rather

$$M_*(t = 0) = \int_0^{14\ \mathrm{Gyr}} \Psi(t)\mathrm{d}t - M_{\mathrm{recy}}(t), \quad (8)$$

where $M_*(t = 0)$ is the stellar mass, $\Psi(t)$ is the SFR such that

$$\int_0^{14\ \mathrm{Gyr}} \Psi(t)\mathrm{d}t = 1, \quad (9)$$

and $M_{\mathrm{recy}}(t)$ is the cumulative gas release.

For each time step the code considers the provided SFH and calculates the amount of mass that is converted from gas into stars and subtracts it from the ISM. The mass of O, Mg, Fe, Si, H, and the total gas released corresponding to the abundance of the ISM at that time is also removed from the ISM and used to calculate the chemistry of the stellar population:

$$\Delta M_{(\mathrm{O,Mg,Si,Fe})} = \frac{\Psi(t)\Delta t}{M_{\mathrm{ISM}}} \times M_{(\mathrm{O,Mg,Si,Fe})}, \quad (10)$$

where $\Delta M_{(\mathrm{O,Mg,Si,Fe})}$ is the mass of O, Mg, Si, or Fe removed from the ISM, $\Psi(t)$ is the SFR, Δt is the time step, M_{ISM} is the mass of the ISM, and $M_{(\mathrm{O,Mg,Si,Fe})}$ is the mass of O, Mg, Si, and Fe present in the ISM.

The code then considers the stars created in every previous time-step and calculates the amount of gas and metals that is returned to the ISM. This is added to the ISM, and the fraction of recycled gas is removed from the stars and returned to the gas component. This is done by interpolating the cumulative yields produced by part A for a stellar population with t = stellar age and a metallicity equal to the formation metallicity. We assumed the instantaneous mixing approximation.

We also kept account of the mass of a stellar population at its formation. This quantity is used at each time step to calculate the mass a population returns to the ISM. The mass of the stellar population taking account of the gas release is simply an output.

Our model therefore differs from standard GCE codes (e.g. Chiappini et al. 1997) in that it is a closed-box model, while other GCE codes assume gradual gas infall over the whole of cosmic time. We have decoupled the SFR from the gas surface density, which other GCE codes implement using a Schmit law (Kennicutt 1983). In our case the SFH is derived purely from fitting the age-[Si/Fe] data with no accretion, while we address the question of fitting the MDF in a separate paper (Haywood et al., in prep.).

3. Setting the scene

3.1. A general scheme

As important as the assumptions in the model is the question of exactly what we wish to model. Data can be diversely interpreted, and one must decide on a general scheme before any modelling.

The scheme we adopted has been sketched out in Haywood et al. (2013) and can be summarised as follows.

We describe the disc of our Galaxy as consisting of two systems, the inner and outer discs, which roughly divide at $R_{\mathrm{GC}} = 7-10$ kpc, the Sun being in the transition zone between the two. This suggestion is different from modelling the Galaxy as one system with properties that vary gradually with Galactocentric radius, as has been described up to now (Chiosi 1980; Chiappini et al. 1997). The data in the solar vicinity reflect the existence of these two systems, and we advocate that two chemical evolutionary paths are necessary to describe the solar neighbourhood content fully.

First path: the inner disc ($R_{\mathrm{GC}} < 7-10$ kpc) is composed of the thick and thin discs[2], which are essentially in continuity, although a marked transition between the two is encoded in the evolution of α-elements and metallicity with age (see Fig. 2). This is a result of a change in the regime of star formation at that epoch (as discussed in Sect. 5). A tight age-metallicity relation has been found in the thick disc (Haywood et al. 2013), testifying that the ISM at this epoch was well mixed. The data show that the chemical evolution continued steadily during a period lasting 4 to 5 Gyr, up to metallicities and α-abundances well in accordance with those of the thin disc 8 Gyr ago. The spread in metallicity visible in the thin-disc sequence, which contrasts with the

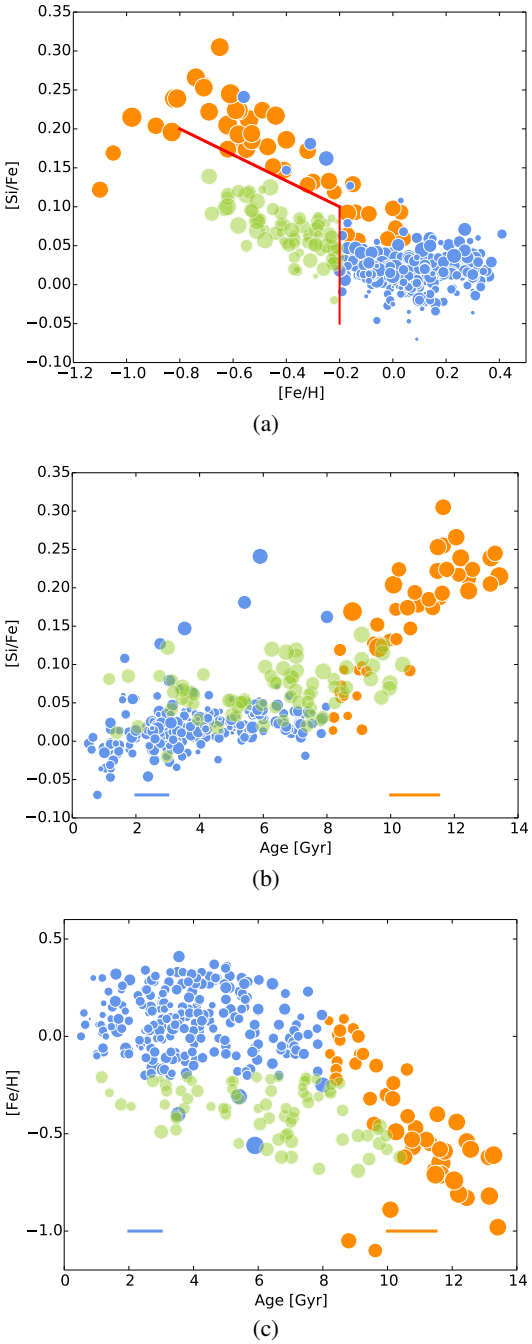

Fig. 2. [Si/Fe] versus [Fe/H] (panel **a**)), [Si/Fe] versus age (panel **b**)) and [Fe/H] versus age (panel **c**)) for the data adopted in this work from Adibekyan et al. (2012) and Haywood et al. (2013). In each panel, the orange points represent thick-disc stars, green points "outer" thin-disc stars and blue points inner thin-disc stars. The red line in panel **a)** shows the selection criterion of outer thin-disc stars as defined in Eq. (12). The size of the points is age for panel **a)**, [Fe/H] for panel **b)** and [Si/Fe] for panel **c)**. The horizontal lines give the estimated error on the ages for young (blue, 1 Gyr) and old (orange, 1.5 Gyr) stars. (This figure is available in color in electronic form.)

[2] Here we refer to the thick and thin discs as the chemical thick and thin discs outlined in Haywood et al. (2013).

tight relation obtained for the thick disc, can be explained by the position of the Sun at the division between the inner and outer disc. This was argued in Haywood et al. (2013), who furthermore elaborated that the simple effects of blurring (radial excursions of stars on their orbits due to epicyclic oscillations) are sufficient to contaminate the solar vicinity with a few percent of stars coming from either the inner or outer regions. This then explains the low- and high-metallicity tails observed in the local distribution. In other words, it is the position of the Sun, at the division of two systems – the inner and the outer disc which have a markedly different chemical history – that can explain the origin of the spread in metallicity observed in the thin disc in the solar vicinity. Hence, as explained in Haywood et al. (2013), we think that no radial migration is necessary to explain the chemical patterns seen in the solar vicinity, see below for additional justifications (end of Sect. 3.2).

Second path: the outer disc ($R_{GC} > 9-10$ kpc) started to form stars 10 Gyr ago, that is, when the thick-disc formation was still on-going in the inner Galaxy. The similarity in α-element abundance between the thick disc and the outer disc at identical ages (∼10 Gyr) suggests that the gaseous material from which the outer disc started to form may have been polluted by gas expelled from the forming thick disc. The substantially lower metallicity of the outer disc stars at those epochs (reaching [Fe/H] ∼ −0.8 dex) compared to the already high metallicity of the thick disc at the same time ([Fe/H] ∼ −0.4 dex) suggests that gas in the outer disc resulted from a mixture of pristine gas present in the outer regions, and gas processed in the inner parts (Haywood et al. 2013).

To summarise, we thus assume that the inner (thick +thin) discs and the outer disc are two systems that can be mostly considered to be the result of two distinct chemical evolution paths and are modelled as such in this paper. In the next section, we present the data with which we compared our model and the main characteristics that our best-fit SFH – and associated chemical evolution – must be able to reproduce.

3.2. Data

The original observations used in this paper are taken from Adibekyan et al. (2012). This was a spectroscopic survey aimed at providing atmospheric parameters and chemical compositions for nearby stars for the purposes of extrasolar planet research. This produced a sample of 1111 stars providing values for temperature, elemental abundances, stellar velocities, and associated errors.

Since our results are derived from fitting the age-α element distribution, *not stellar densities*, no bias due to the volume definition of the sample is expected. Three other biases might be important, however: the first is due to the measured abundances. More than any other sample, we expect this one to have excellent abundance measurements because of the very high signal-to-noise ratio advocated in Adibekyan et al. (2012). Moreover, comparison of abundances with other recent spectroscopic samples agree well. The second type of bias could come from the age estimates. The uncertainties for the ages – both systematic and random – were estimated in Haywood et al. (2013), and we refer to Haywood et al. (2013) for the full details of how the ages were derived for the sample. We provide a brief summary here, however. Individual stellar ages were derived using the Bayesian method of Jørgensen & Lindegren (2005), adopting the Yonsei-Yale (Y2) set of isochrones (version 2, Demarque et al. 2004). Haywood et al. (2013) estimated that the uncertainties in the atmospheric parameters translate into uncertainties of about 0.8 Gyr for the younger stars (age < 5 Gyr) and 1.5 Gyr for the oldest (age > 9 Gyr). Because systematic errors on the effective temperature scale induce large errors on the derived ages (see Haywood 2006), the effective temperatures from Adibekyan et al. (2012) were also checked against the $V - K - T_{\rm eff}$ scale from Casagrande et al. (2010). An attempt to estimate systematics from the uncertainties in stellar models (by adopting another set of isochrones) and method (Bayesian estimate compared to χ^2 fitting) was also carried out and yielded absolute (systematic) uncertainties of 1 to 1.5 Gyr and random uncertainties of 0.8 to 1.5 Gyr. The final source of potential bias we considered might be induced by incomplete coverage of the α-elements over the whole age interval. However, within the age interval considered here, the age-α relation is extremely well defined. A consequence of this, however, was a severe pruning of the sample to keep only the best ages.

The sample of Adibekyan et al. (2012) was used by Haywood et al. (2013) to derive ages for a cleaned sample of 363 stars with their associated error estimates.

In their paper, Haywood et al. (2013) developed a scenario where the Galaxy is composed of several distinct components, an inner and outer thin disc, and a thick disc. Their interpretation has been discussed extensively in the previous subsection and is modelled and tested in this paper.

In Fig. 2 we show the distribution of stars by comparing [α/Fe] vs. [Fe/H], [α/Fe] vs. age and [Fe/H] vs. age. We differentiate the inner (thick and thin) disc and outer disc.

We used silicon to follow the α-element evolution. The reason we chose this element and not the α as defined by Haywood et al. (2013) is that the abundance ratios of the various α-elements are much higher for the theoretical yields than in the observations. This means that using α as described in Haywood et al. (2013) is not possible using Anders & Grevesse (1989) solar normalisations. Thus, we were unable to use the definition of α used in Haywood et al. (2013), and do not expect much agreement between the chemical tracks of the different α-elements. Silicon is, however, different from other α-elements, such as magnesium, in that it is produced in significant quantities by both SNII and SNIa. This is an important difference because more of the α total value is produced in a few Myr for magnesium, while the stars release silicon over longer time-periods.

The [Si/Mg] value is significantly higher when using the theoretical yields than in the data (assuming Anders & Grevesse (1989) solar values). We chose silicon because, for this element, our model can fit the [α/Fe]-age distribution and the [α/Fe]-[Fe/H] distribution using the same SFR. This inability to match the magnesium evolution to the data may be due to either shortcomings in the model itself or the theoretical yields. However, although several GCE papers (e.g. François et al. 2004) have studied several elements and compared them to data, they tend to only fit the [α/Fe]-[Fe/H] distribution and not to the level of precision we require[3]. Silicon allows us to achieve a good fit to the data, while the other elements tend to fail to produce a fit in [α/Fe]-age-[Fe/H].

We discuss in greater detail the reason for choosing to follow silicon rather than an alternative α-element in Sect. 6.5.

[Si/Fe] versus [Fe/H] relation

In the [Si/Fe] vs. [Fe/H] plane (Fig. 2, panel a), the inner thick and thin discs still show two distinct patterns, with the thick

[3] A stringent test of the chemical yields is beyond the scope of this paper.

disc forming a sequence of decreasing [Si/Fe] for increasing metallicities. At the end of this sequence, for [Si/Fe] ∼ 0.05 dex and [Fe/H] ∼ −0.1 dex, the thin disc appears as a nearly flat track, with nearly constant [Si/Fe] values (with a mean around solar) and [Fe/H] between –0.2 dex and 0.4 dex. The low-metallicity tail of the thin-disc sequence ([Fe/H] < −0.2−−0.3 dex) is the locus of outer disc stars. Interestingly, these stars have [Si/Fe] values higher than those characterizing inner thin-disc stars, reaching 0.15 dex. This places the outer disc at an intermediate sequence (in α-abundance) between the thick and thin discs.

As anticipated, we separated the outer disc and treat it as a separate component from the point of view of chemical evolution. Formally, outer disc stars are defined as those that lie inside the region defined by the relation

$$[\mathrm{Si/Fe}] < -[\mathrm{Fe/H}]/6. + 1/15.\ \mathrm{dex} \quad (11)$$

$$[\mathrm{Fe/H}] < -0.2\ \mathrm{dex} \quad (12)$$

shown in Fig. 2, panel a.

These limits are somewhat arbitrary. A justification a posteriori (which came after this work was submitted) for this choice comes from the APOGEE survey (Nidever et al. 2014), which has confirmed the scheme presented by Haywood et al. (2013) that the outer and inner disc are the result of two different paths of chemical evolution, as is modelled here. The APOGEE data clearly show that the inner-disc stars of solar α-abundance essentially have a metallicity higher than −0.2 dex (see. Fig. 11 of Nidever et al. 2014 or Fig. 14 of Anders et al. 2014). We give more details on the origin of the stars in our sample below.

[Si/Fe] versus age relation

The thick disc consists of stars with ages greater than 8 Gyr and shows a rapid evolution of [Si/Fe] with time, almost 0.3 dex in 6 Gyr (see Fig. 2, panel b). The idea that the ISM is well mixed is indicated by the low scatter in [Si/Fe] with age for old stars in the thick disc (Fig. 2, Haywood et al. 2013; Adibekyan et al. 2012).

The (inner) thin disc consists of stars younger than 8 Gyr, and its [Si/Fe] evolution vs. time is significantly flatter than that of the thick disc, only about 0.05 dex over 8 Gyr. A key characteristic of the transition between the thick and thin discs in the [Si/Fe] vs. age plane is that it is apparently very sharp. It forms a knee where the gradient of [Si/Fe]-age evolution drops very suddenly.

Finally, the oldest stars in the outer disc form at approximately 10 Gyr and evolve parallel to the inner thin disc, but with a higher [Si/Fe] ratio. It is as if the outer disc turned off the thick-disc sequence earlier than the (inner) thin disc.

[Fe/H] versus age relation

After outer disc stars were separated from inner disc stars, the thick-disc sequence appears in the [Fe/H] vs. age plane (Fig. 2, panel c) as a well-defined track. This track is characterised by a small scatter around the mean value for all ages between 8 and 13 Gyr. As extensively discussed in Haywood et al. (2013), the metallicity homogeneity that characterises the thick-disc phase can be interpreted as the signature of an intense episode of star formation at these times. As a result, the feedback from SNe explosions efficiently mixed metals, and assured a homogeneous ISM during the whole phase of thick-disc formation. This efficient mixing must also have limited the formation of any radial metallicity gradient: the small scatter around the mean [Fe/H] vs. age relation of the thick disc is evidence that any gradient, if present, must have been weak, otherwise the spread in the relation would appear much higher (Haywood et al. 2013).

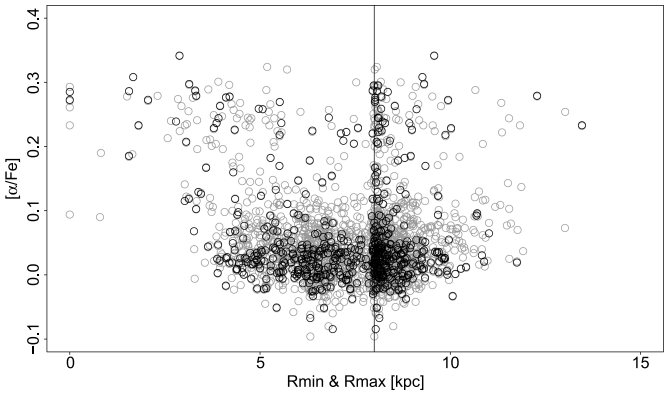

Fig. 3. Pericentres (at R < 8 kpc) and apocentres (at R > 8 kpc) vs. [α/Fe] for stars in the sample of Adibekyan et al. The stars with age determinations used here are shown in black. The data illustrate that the thick-disc stars at [α/Fe] > 0.2 dex span the whole range of radii from the Galactic centre to ∼10 kpc.

The signature of the existence of a steep metallicity gradient in the transition zone (7−9 kpc) between the inner and outer thin disc is imprinted on the significant scatter observed in the [Fe/H] vs. age relation at ages < 8 Gyr. The APOGEE survey (see Anders et al. 2014; Nidever et al. 2014) has shown that stars with [Fe/H] > +0.2 dex and [Fe/H] < −0.2 dex are present at just R < 7 kpc and R > 9 kpc, which explains why simple blurring can bring these stars to the solar orbit.

The outer disc, as already noted in the [α/Fe] vs. age plot, starts to appear about 10 Gyr ago at metallicities ∼–0.7 dex. Its subsequent [Fe/H] pattern is always below that characterising the inner thin disc. The metal enrichment proceeds in the outer disc at a rate similar to that of inner disc stars, reaching values of about −0.3 dex for ages <2 Gyr.

Origin of the stars

Figure 3 shows the α-abundance of the stars in the sample as a function of their pericentre (at R < 8 kpc) and apocentre (at R > 8 kpc). The orbits of the stars were computed from U, V, W velocities provided in the catalogue of Adibekyan et al. and an axisymetric potential from Allen & Santillan (1991). The mean orbital parameters were derived from orbits integrated for 5 Gyr. The figure illustrates that thick-disc stars are present at all radii, from the Galactic centre to about 10 kpc, confirming that stars in the solar vicinity probably originated across a broad range of radii. Note that, contrary to other studies, we did not assume that (thick or thin) disc stars have migrated. In addition to the detailed justifications given in Haywood et al. (2013), Fig. 3 clearly shows that thin-disc stars have pericentres that bring them to distances of less than 5 kpc from the centre (towards the Galactic centre) to distances of more than 9 kpc (towards the anticentre).

The metal-poor stars are characterised by their tendency to travel along their orbit faster than the local standard of rest (LSR), as shown in Haywood (2008) – whereas the thick disc, at the same metallicities, lags the LSR.

These stars have been characterised on larger orbits, see Bovy et al. (2012), Fig. 7, which shows that these objects have average guiding centers larger than the solar radius (R_{mean} > 9 kpc).

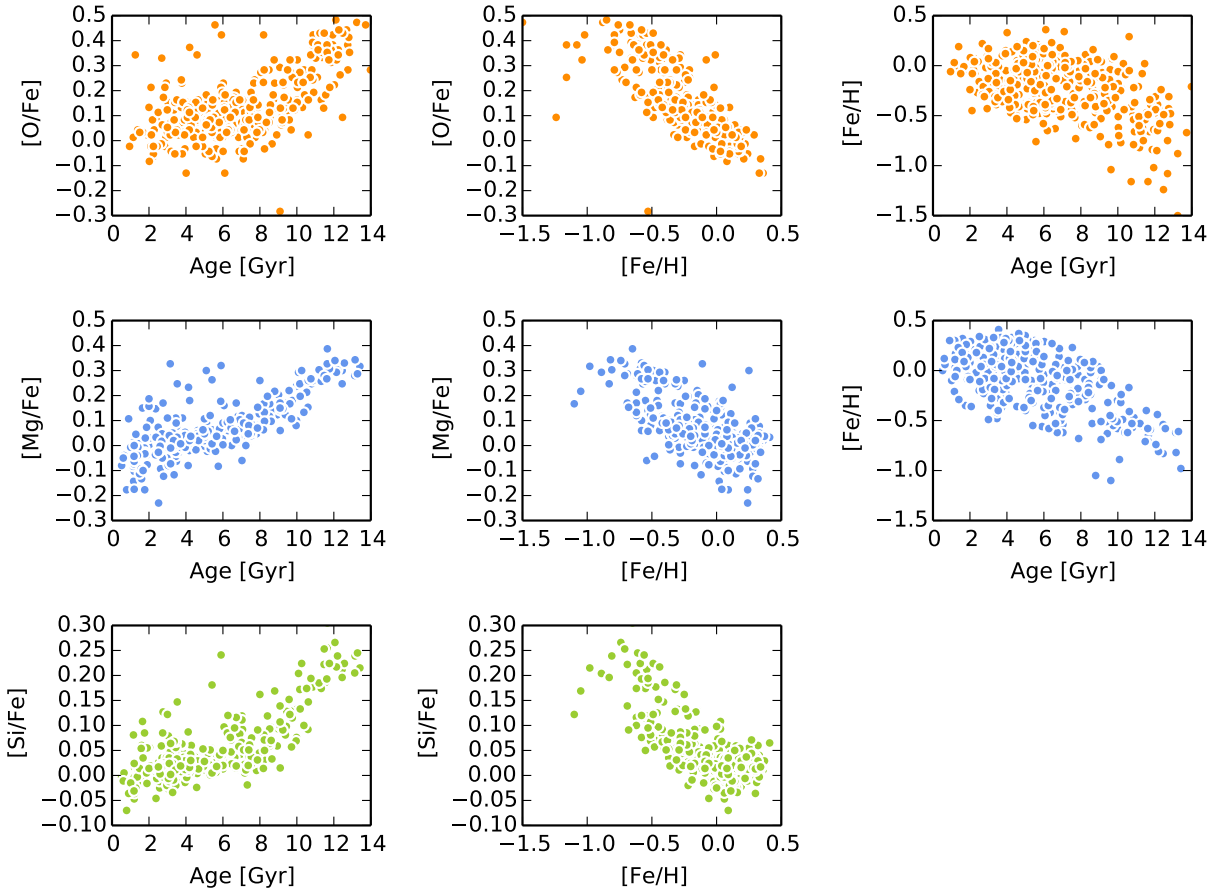

Fig. 4. Comparison of the different α species and datasets. From *top to bottom* we show the oxygen data from Ramírez et al. (2013) (orange) and the magnesium (blue) and silicon (green) data from Adibekyan et al. (2012) and Haywood et al. (2013). The columns are for age-[α/Fe], [Fe/H]-[α/Fe] and age-[Fe/H] distributions. The [Fe/H]-age distributions are the same for silicon and magnesium, therefore we only show them once.

3.3. The sample of Ramírez et al. (2013)

We have mentioned above that we chose silicon as our marker for the α-abundance for most of this paper. Figure 4 compares silicon, magnesium and age from Adibekyan et al. (2012) and Haywood et al. (2013) with the oxygen abundances and ages presented in Ramírez et al. (2013) for a sample of 391 FGK dwarfs and subgiants from the solar vicinity. The mean error in age is of the order of 2−3 Gyr and about 0.05−0.06 dex on [O/Fe], as quoted by the authors. The remarks concerning possible biases in our sample also apply to Ramírez et al. (2013). The oxygen data are more scattered than silicon and magnesium, because of the larger uncertainties. The data with the tightest correlations clearly belong to silicon. However, the key features of the [α/Fe] evolution is visible in each plot. We see a steep early-time slope with very little scatter followed by a sharp transition to a shallower slope. Unfortunately, the split between inner and outer discs visible in the [α/Fe]-[Fe/H] distribution of the dataset of Haywood et al. (2013) cannot be seen for the Ramírez et al. (2013), but the change of slope due to the transition from thick to thin disc in oxygen abundance is clearly seen at about 8 Gyr, although the spectroscopic data, elements, and ages are different.

4. Impact of star formation histories on chemical abundance patterns

Over the next few years a wealth of high-quality spectroscopic data together with highly accurate measurements of stellar ages are expected as a result of on-going spectroscopic surveys and the *Gaia* mission.

These data are expected to allow us to measure the evolution of most chemical species in the Milky Way in detail and thus reconstruct the SFH of the Galaxy. However, we still have very little knowledge about which processes generate the chemical abundance patterns observable in a galaxy. The features in the abundance data for the Galaxy are usually only discussed qualitatively or over a restricted range of parameters that are tuned to fit solar neighbourhood data.

In this section we describe how the chemical evolution of the model is affected by the SFH we provide. We explore how the various parameters and ingredients generate, and affect, the chemical patterns that result.

4.1. Exponential SFR

We start by using an SFR with an exponential distribution of the form

$$SFR(t) = A \exp(-t/\tau), \tag{13}$$

where t is the time in Gyr since the beginning of the "universe", τ is the characteristic time scale, and A is a constant. We vary A so that the total mass of stars formed over the whole time interval is equal to 1, meaning that in the absence of recycled gas from stellar evolution, all the ISM is consumed. We vary the value of τ between 1 Gyr and 10 000 Gyr so that the SFR ranges

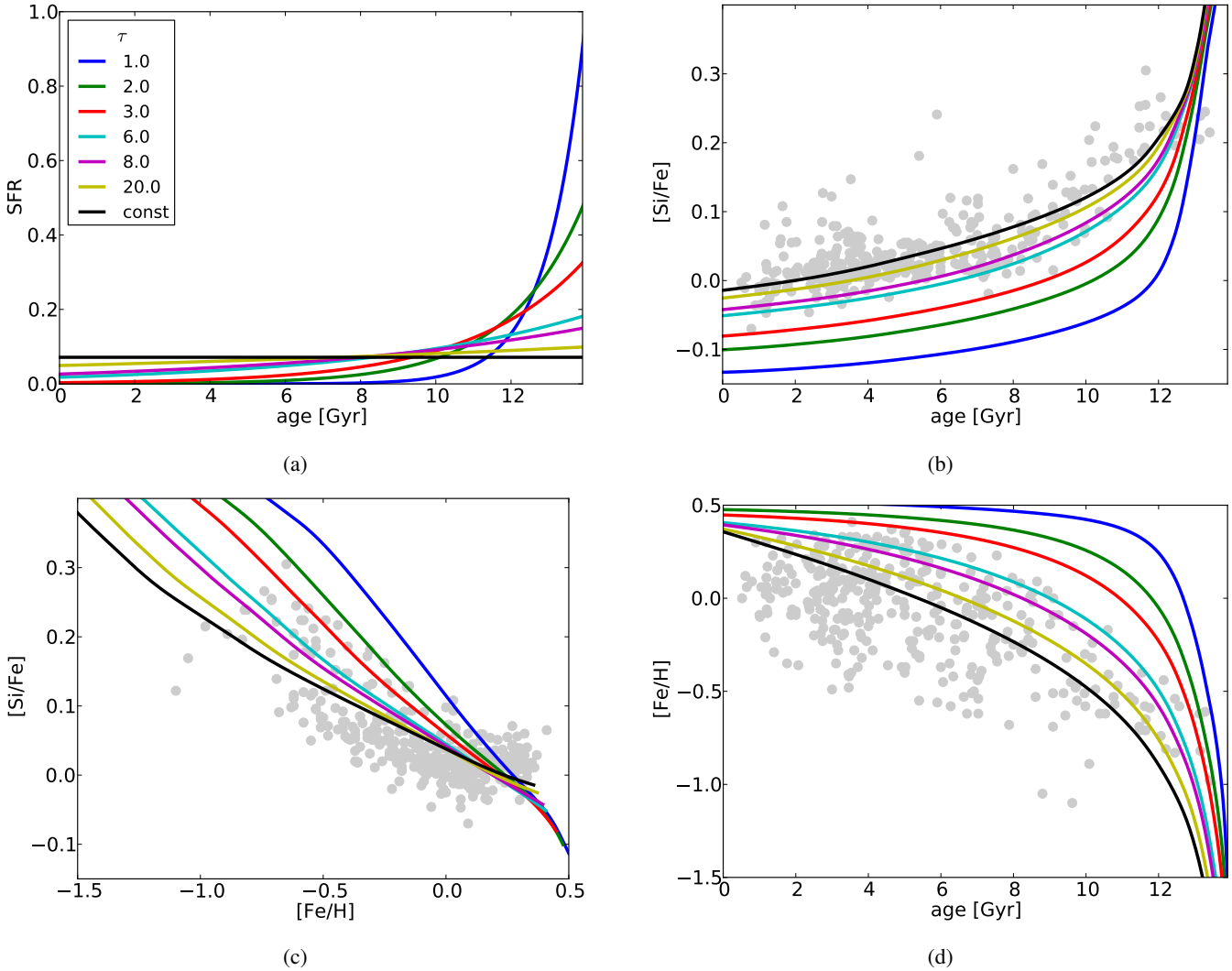

Fig. 5. Chemical evolution tracks in the [Si/Fe] vs. age (panel **b**)), [Si/Fe] vs. [Fe/H] (panel **c**)) and [Fe/H] vs. age (panel **d**)) planes, produced by exponential SFRs, with different τ time scales, (panel **a**)). The grey points are the solar neighbourhood data from Haywood et al. (2013) and include both inner and outer disc stars.

from a very high initial value followed by a rapid decline to an essentially constant function (see Fig. 5, panel a).

We chose an exponential form for the SFR at this stage because it is a simple function and closely mimics the most commonly occurring forms in the literature, see Matteucci & Francois (1989), Chiosi (1980), Chiappini et al. (1997), and Fenner et al. (2002) for an SFR based on the surface density of infalling gas and the Schmidt-Kennicutt relation (Kennicutt 1998).

From Fig. 5 we can deduce some important features of the evolution of the SFR and the chemistry:

1. A high initial SFR followed by a rapid decline (e.g. $\tau = 1$) induces a rapid fall in the [α/Fe] ratio, while higher values of τ produce a more gentle decrease of the [α/Fe] ratio with time.
2. A low τ SFH also generates a too rapid enrichment in [Fe/H], such that the metallicity reaches solar values after only about 1 Gyr. Such a rapid increase in the metal content for low τ values is also the cause of the rapid decrease in [α/Fe] discussed in the previous point.
3. The higher the characteristic time, τ, the closer the corresponding tracks are to the [Si/Fe] and [Fe/H] versus age data (see panels b and d). The constant SFR, in particular, seems a good solution that reproduces the chemical patterns as a function of age reasonably well. However, it is able to reproduce neither the thick disc nor the thin disc sequence in panel c.
4. In the age-[Si/Fe] plot (panel b) it is clear that the knee feature that can be seen in the data (Fig. 2) is most evident in the model tracks where the initial SFH is large and the sharpness of the contrast between the early and late SFR is greater. This suggests that a sharp transition is required in the SFH of the Galaxy to mimic the chemical abundances of the stars described in Adibekyan et al. (2012), and that the contrast between early- and late-time Galactic SFR must be considerable.
5. In most GCE models the [α/Fe]-[Fe/H] distribution (as in our panel c) is used to test the conformity of models to observations. There is considerable variation in the tracks followed by the model in [α/Fe]-[Fe/H] space as a result of changing τ. The figure clearly shows that a wide range of τ values are a fairly good fit to the data. More specifically, panel c shows that SFHs with characteristic times τ between 3 and 6 Gyr pass through the thick- and thin-disc sequences, with

Table 1. Parameters for the different SFH shown in Fig. 6.

	Gaussian		Other		
Name	μ	σ	Gap width	Gap position	c
basic	0.5	1.0	0.	N/A	0.30
low C	0.5	1.0	0.	N/A	0.01
peak shift	3.0	1.0	0.	N/A	0.01
thin peak (a)	0.5	0.2	0.	N/A	0.01
+gap	0.5	1.0	1.	9	0.01
thin peak (b)	0.5	0.2	0.	N/A	0.01

Notes. The SFH consists of a Gaussian peak, with μ and σ corresponding to the mean and width of the peak (see Eq. (14)). Low C indicates that the constant part of the SFH has a low value. The thin-peak SFRs (a and b) change the width of the peak. Thin peak (a) shows an SFH where the peak is narrow and the height of the constant part is the same as for the basic case. Thin peak (b) is where the constant is adjusted so that the mass fraction formed in the peak is the same as for the basic case.

$\tau = 3$ perhaps the best solution. However, none of these values can adequately represent the sequences in the [Si/Fe]-age and [Fe/H]-age plane. This indicates that [α/Fe]-[Fe/H] patterns are not sufficient to distinguish the SFH of the Galaxy and that the knowledge of ages is essential for this purpose.

We note that the $\tau = 6$ Gyr SFR is the steepest exponential allowed by the data. If more stars are formed at earlier times, then the line no longer passes through the [Si/Fe]-age distribution or the upper sequence of the [Si/Fe]-[Fe/H] panel. Choosing $\tau = 6$ results in an evolution of [Fe/H] with age that covers the top envelope of the data.

However, the exponential functional form does not fit the old thick-disc stars in panel b. The [Si/Fe]-age evolution of the Milky Way data can be fit by two straight lines plus a knee. This is not what we see in the chemical tracks generated by exponential SFRs, because the change in slope is much more gradual. This discrepancy suggests that another functional form is more appropriate.

4.2. A more complex SFR

In Fig. 6 we show the various forms of a more complex SFH. We chose a form consisting of an initial burst of star formation, modelled with a Gaussian, followed by a quiet period, modelled using a constant SFR. This SFH is of the form

$$SFR = \begin{cases} \exp(-(t-\mu)^2/2\sigma^2) & \text{if} \quad SFR > C \quad \text{and} \quad t < \mu \\ C & \text{otherwise,} \end{cases} \tag{14}$$

where t is the stellar age, μ is the position of the peak in Gyr, σ is the width of the Gaussian, and C is the height of the constant part of the SFH. We also allow for the existence of a gap in the SFR such as the one introduced by Chiappini et al. (1997). This functional form is more similar to the SFRs recovered by some ΛCDM cosmological simulations (e.g. Brook et al. 2014; Stinson et al. 2013; Aumer & White 2013). Table 1 shows the various parameters used for the different SFHs adopted in Fig. 6. These parameters were chosen to provide, as as much as possible, an overview of the different chemical features produced by SFHs of this type.

Table 2. Summary of the parameters used in Sect. 5.

Yields	
SNII	Nomoto et al. (2006)
AGB	Karakas (2010)
SNIa	Iwamoto et al. (1999)
IMF	Kroupa (2001)
Solar abundances	
Si	7.55 (Anders & Grevesse 1989)
Fe	7.51 (Anders & Grevesse 1989)

While none of these SFRs is a good representation of the data, we can see that

1. Many of them reproduce a "knee" feature in the [Si/Fe] vs. age plot (panel b) and the timing of the knee appearance is related to the end of the burst phase (described by the Gaussian). Moreover, the higher the ratio between the peak of the SFR in the burst phase and the value in the constant SFR regime, the sharper the knee feature. There is no sign of such a feature in the lower τ SFRs in Fig. 5.
2. The knee arises when the SFR, and thus the SNII rate, falls rapidly or becomes zero (for example the cyan line in Fig. 6). When this occurs, the contribution of silicon from the SNII is reduced within a few Myr (essentially in step with the SFR), but because of the longer time-delay distribution for SNIa, the iron continues to be produced at almost the same rate for over a Gyr. Thus, the amount of iron continues to build up as a result of SNIa from stars that have previously formed. Only when the SFR subsequently increases do the α-elements start to enrich the gas again. This causes a drop in the [Si/Fe] and thus makes the knee sharp.
3. A delayed star formation burst (peaking at $t \sim 9$ Gyr) implies too high [Si/Fe] values for the whole thick-disc phase and also a too slow metal enrichment. The delayed star forming burst does, however, fit the metallicity-[Si/Fe] distribution (panel c).
4. A 1−2 Gyr halt in the star formation causes a decrease in the [Si/Fe] values at about the same time, as well as a local minimum in the [Fe/H] vs. age plot. The reasons for this are outlined in point 2.
5. The data are essentially bracketed by SFRs that have an initial peak of star formation at $t = 9$ Gyr and $t = 13.5$ Gyr: both fit the [α/Fe]-[Fe/H] (panel c) sequence, but provide too low or too high α values and metallicities in the thick-disc phase. However, the thin-disc phase is fitted equally well for both observables.

From these experiments, it is clear that changing the SFH has a considerable effect on the chemical evolution of a galaxy. Moreover, as already noted in Sect. 4.1, using a [α/Fe]-[Fe/H] distribution alone is not sufficient to properly distinguish between different SFHs. For a good comparison between models and data age information is required.

5. Reconstructing the SFR of the Milky Way

Based on our exploration of the effect of a given SFR on the chemical abundance history, we now attempt to use the chemical evolution of the Galaxy, as traced by Haywood et al. (2013), to recover the SFH. After describing our fitting procedure, we first derive the SFH of the inner (thick+thin) disc, then that of the outer disc. We assume the inner and outer discs to be two

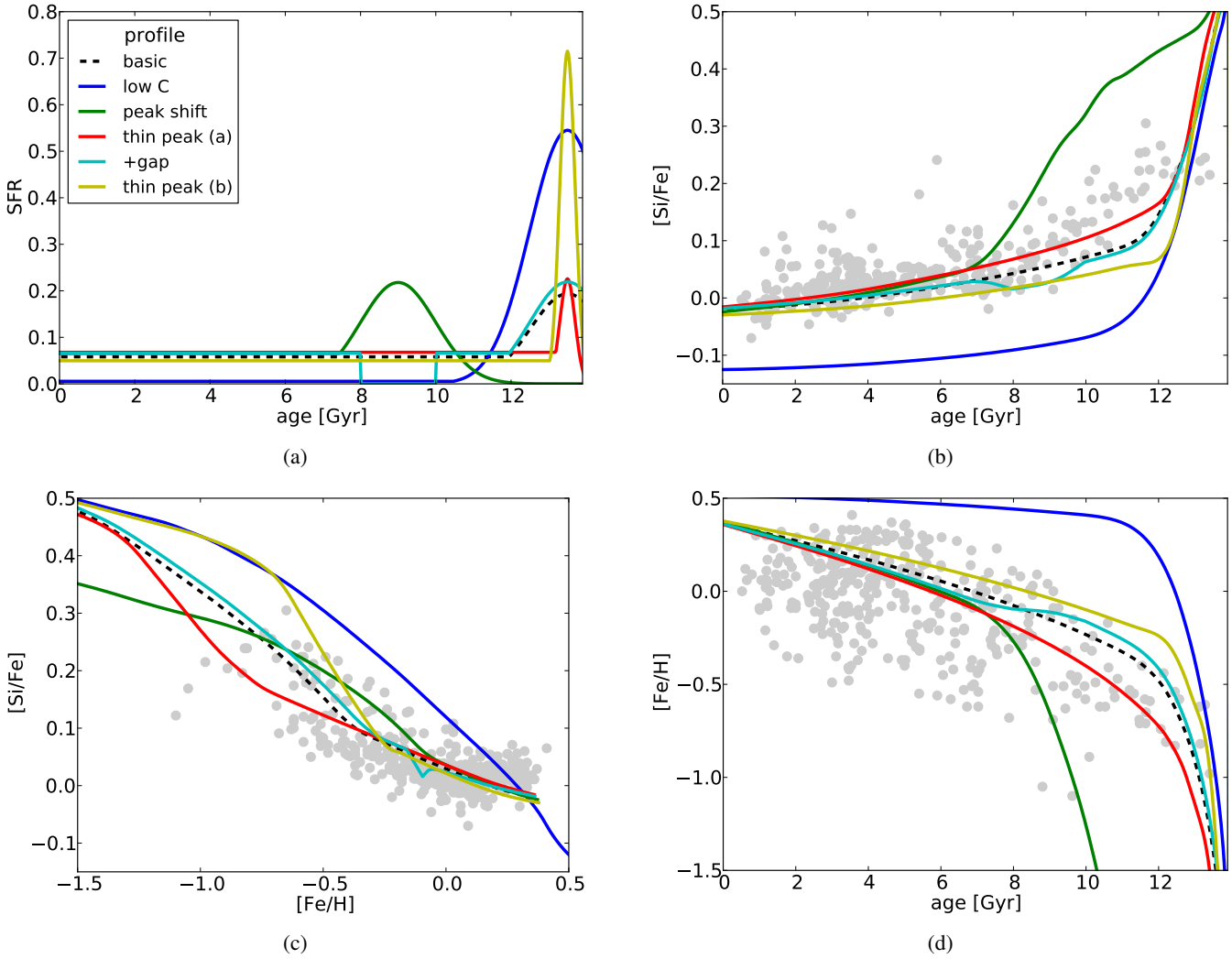

Fig. 6. Chemical evolution of the model depending upon a selection of different SFHs (panel **a)**, Table 1). Panels **b)**, **c)** and **d)** show the evolution of [Si/Fe] with age, [Si/Fe] with metallicity, and the metallicity with age. The grey points are the data from Haywood et al. (2013), including inner and outer disc stars.

systems that evolve independently, as described in Sect. 3. The properties and ingredients of our model are given in Table 2. The solar iron normalisation is the "best" value for the iron normalisation and is not the one used to normalise the data from Adibekyan et al. (2012) (the value used there is 7.47 based on Gonzalez & Laws 2000). It matches Anders & Grevesse (1989) and allows a very good fit to both the age-[Si/Fe] and metallicity-[Si/Fe] distributions.

5.1. Fitting procedure

To recover the SFH of our Galaxy in the last 13 Gyr, we have chosen to fit the evolution of [α/Fe] with age. This choice is motivated by the fact that this relationship is much more dependent on the SFH than the [α/Fe]-[Fe/H] distribution (Fig. 6).

As shown in the previous section (see Fig. 5), two SFHs are likely to bracket all other possible tracks: the constant SFR, and a sharp initial burst containing the vast majority of the star formation, which results in a very rapid increase in the metallicity and a sharp decrease in the [α/Fe] distribution. We found that of the three elements we chose to follow (silicon, magnesium, and oxygen) only the silicon and oxygen chemical tracks generated by these two limiting SFHs bracket the observed abundances when adopting the same (meteoric) solar abundances used in the data. For this reason, and because oxygen data is considerably noisier than silicon, we deduced the SFH from fitting our model to the evolution of [Si/Fe] with age.

Our fitting procedure is based on a simple χ^2 approach. The algorithm requires an initial-guess SFH and a user-supplied convergence criterion. For our initial condition we used an SFH defined by the function

$$f(t) = A/(0.01t + 0.1), \tag{15}$$

where A is the normalisation and t is the time. We also tested other SFH forms, such as a sharp initial burst, constant star formation, or a high initial SFR followed by a linearly declining SFR. The SFHs all converge to the same result, except for the constant SFR. The constant SFR converges to *almost* the same age-[Si/Fe] distribution and final SFH, but it lacks the dip and therefore the sharp break in the age-[Si/Fe] track. However, using an alternative fitting algorithm (Powells algorithm, see Fig. 11), this difference vanishes. This algorithm seems more robust when fitting, but takes considerably longer to converge.

We divided the age range (0−14.0 Gyr) into 28 nodes separated by 0.5 Gyr and used a χ^2 fitting procedure to calculate the SFR. After providing an initial SFH, we allowed minimisation to

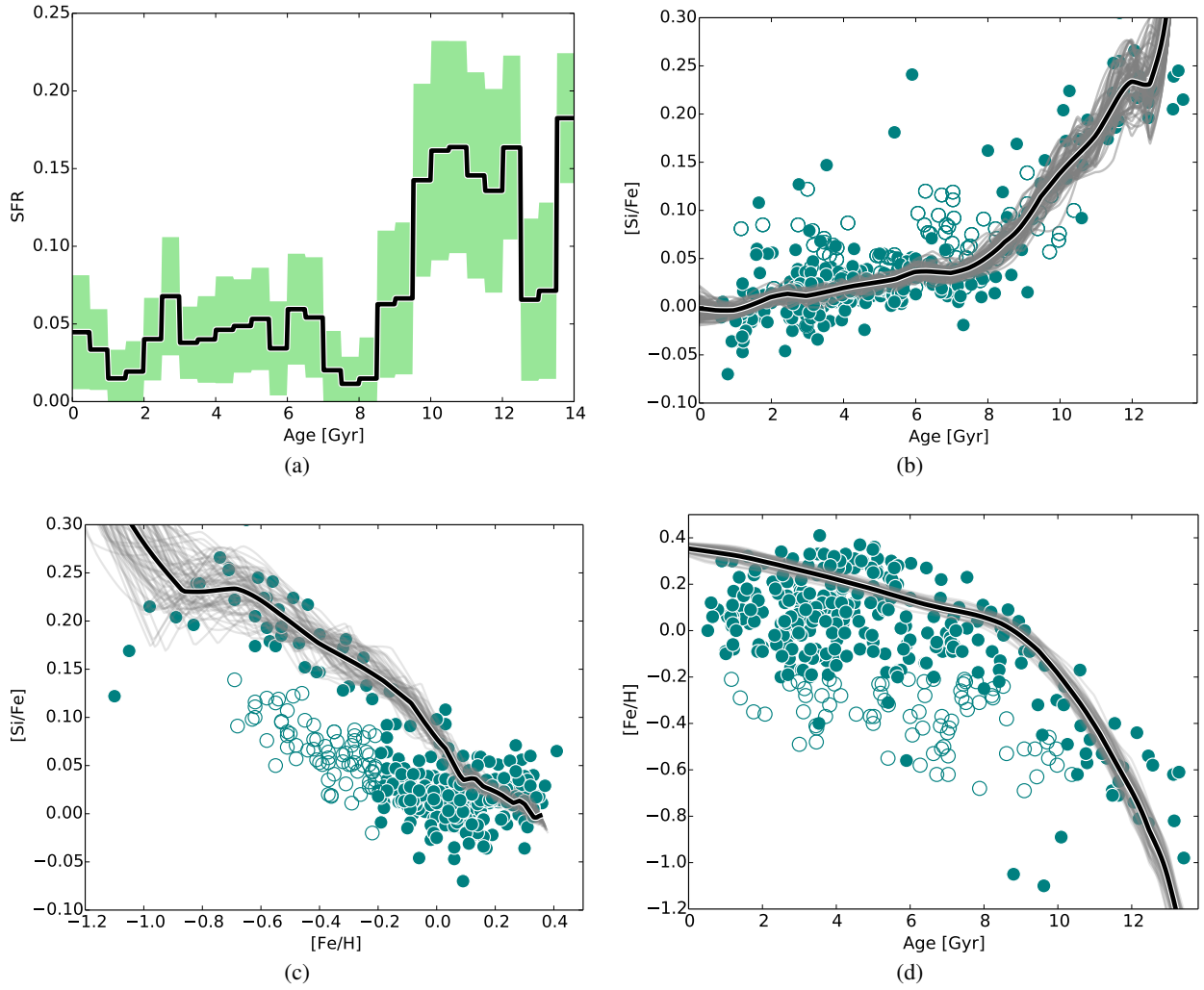

Fig. 7. Chemical evolution of the best-fit SFH for silicon of the inner disc using the solar abundances of Anders & Grevesse (1989). The grey lines are the results of the various bootstrapped best-fit SFHs, the black line is the mean value. Filled circles are the inner disc stars, empty circles are the outer disc from Haywood et al. (2013). In panel **a)** the green region is the standard deviation on the values in each bin. These values are not independent and the variance in the total SFH is considerably smaller than in each individual bin. Panels **a)**–**d)** show the best-fit SFH, the evolution of [Si/Fe] with age, the evolution of [Si/Fe] with metallicity, and the evolution of the metallicity with age.

take place using this initial guess. At each iteration an entire SFH was created, and the chemical evolution code was used to calculated the corresponding chemical track. We then calculate the χ^2 value using the difference between the model value of [Si/Fe] at the age of each star in the data and the observed [Si/Fe] for all stars with ages lower than 13 Gyr. We set this maximum age limit because there are very few stars with ages greater than this, and so this region is difficult to constrain reliably.

The algorithm uses an N-dimensional simplex and follows a series of steps, attempting to find a minimum. Convergence is considered to be where a step of the algorithm is smaller than a given minimum, or that the decrease in χ^2 is lower than a given value.

When a best fit SFH was found using the whole data sample, we used a bootstrap procedure to quantify the sensitivity of the SFH to the data. We then averaged the various solutions obtained to smooth the SFH.

As discussed previously, we normalised the SFH such that initially the ISM has a mass of 1 and, over the 14 Gyr of evolution the integral of the SFH is equal to one. This means that without gas release the total mass of stars would be unity, and the mass of the ISM would be zero. However, because gas is released from stellar populations over time, the final gas mass is not zero, and the final stellar mass is not one. After 14 Gyr, the total mass present in the ISM is equal to the mass of gas released from the stars. That is not to say that all the gas present has been recycled through stars, because at each stage the gas and metals released are mixed with the ISM. However, at all times, the total baryonic mass (gas and stars) in the system is one. When the total amount of star formation is fixed, the only freedom in the system is the actual form of the SFH, not the total amount of stars formed.

5.2. Inner discs: thick and thin

The SFH resulting from fitting the [Si/Fe]-age sequence of inner disc stars is given in Fig. 7 (panel a). We show the results of each bootstrap, the mean recovered SFR, and an estimate of the variation in each bin in panels b, c, and d. It is important to note that while there is considerable variation in each bin (green shaded area), the shape of the overall SFH is more constrained. The spread of SFRs in each of the 28 bins shown in panel a is not independent, and is more constrained globally than in each individual step.

We can immediately see various features of the SFH of interest.

- Because we sampled stars from across the entire Galactic disc and fitted their evolution, we conclude that the thick-disc phase SFR is three times more intense than the thin-disc phase. We therefore expect that the thick disc (formed from stars with ages between 8 and 13 Gyr) contains about 56% of the total stellar mass of the Milky Way. We emphasize that this is a *ratio* of thick-to-thin-disc SFRs across the discs and not an absolute value.
- We can also see a dip in the SFR for about 1 Gyr at around 8 Gyr, which is required to form the sharpness of the knee between the two slopes. We note that although is it a common feature of GCE codes – in which it tends to occur earlier (e.g. Chiappini et al. 1997) – this is the first time that it was measured from chemical data. This dip indicates that some process is required to re-initiate star formation at later times. Our model cannot suggest what event causes this, although suggestions include external gas accretion or the cooling of hot gas to restore a depleted cold gas reservoir.
- The mean SFH in the thin-disc phase (age < 7 Gyr) is compatible with a constant SFR at the level of 4.7 solar masses per year if our total SFH is normalised to the total Milky Way stellar mass from McMillan (2011). This is compatible with the SFR measured in the young disc (Diehl et al. 2006; Robitaille & Whitney 2010) of between 4 $M_{\odot}$/yr and 1.4 $M_{\odot}$/yr. The last Gyr of star formation is the most poorly constrained because of lack of stars and because any given feature in the SFH only affects stars formed after it. This means that old stars have a stronger effect on the chemical evolution than young stars.
- The error bars reflect the fluctuations in the fitting caused by the varying sample sizes along the [Si/Fe]-age distribution. The [Si/Fe]-age distribution is less populated in the thick-disc phase where the error bars are larger. However, our metallicity is less sensitive to the SFR than in a GCE model that includes infall because there is a more substantial ISM in which to dilute the metals in our model.
- Panel c shows the model [Si/Fe] vs. [Fe/H] track compared to the data. In the thick-disc regime (for [Si/Fe] > 0.05 dex), the model describes the [Si/Fe] vs. [Fe/H] sequence perfectly. Note that although the variation of [Si/Fe] vs. [Fe/H] in the thick disc is de facto a temporal sequence, this is much less the case for thin-disc stars, where the variation of [α/Fe] with metallicity reflects the contamination of the solar vicinity by stars of the inner and outer disc of all ages, not an evolution. *Therefore, the model is not expected to represent the variation seen in the data in the thin-disc regime.*
- The recovered SFH also fits the age-metallicity relation nicely, except for very young ages (<2 Gyr). The relation obtained is above the data. This may be due to the fact that there are only few stars with ages younger than 2 Gyr to constrain the late chemical evolution and that when the stellar Z is greater than 1 $Z_{\odot}$, the yields are extrapolations.
- The model recovers similar features for each bootstrap, except for some noise. The chemical evolution tracks are much narrower than the SFR, with only slight variations, thus illustrating that the chemical evolution is not as sensitive to short variations in the SFR, but to the overall shape of the SFH.

Figure 8 shows that at the end of the evolution, the amount of recycled gas is 30%. This corresponds to the idea that of total amount of stars formed during the whole evolution of the system (1, in normalised units), only 70% is still locked in stars (or stellar remnants such as white dwarfs, black holes, etc.) at the end. The remaining 30% has been recycled as gas in the ISM. This recycled gas fraction depends closely on the chosen IMF, and the quoted value is for the Kroupa (2001) IMF. Other IMFs can give noticeably different values, for example, a Scalo (1998) IMF produces a recycled gas fraction of around 40%. This is discussed more extensively in Sect. 6.

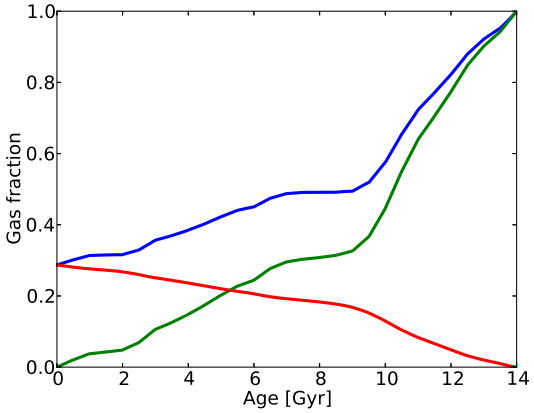

Fig. 8. Evolution of the gas fraction with time resulting from the mean SFH given in Fig. 7. The blue line is the net fraction of gas in the system with time, the red line shows the fraction of recycled gas from stars, while the green line shows the evolution of gas fraction in the absence of gas recycling.

5.3. Outer thin disc

The oldest metal-poor thin-disc stars seen in the solar neighbourhood have ages of 9−10 Gyr and metallicities of [Fe/H] ∼ −0.6 dex (see Haywood et al. 2013). They have similar levels of α-element enrichment as thick-disc stars of the same age, but a noticeably lower metallicity (at least 0.4 dex lower). While the origin of these differences needs to be fully understood, it was suggested in Haywood et al. (2013) that these lower metallicity stars result from outflows of enriched gas coming from the forming thick disc and pristine, accreted gas falling in from the outer halo. In other words, metals coming from the inner disc may have been diluted by more pristine gas coming from the halo, with the outer thin disc starting to form stars at a look-back time of 10 Gyr. So that contrary to what has been adopted for the inner disc, we assume that the initial metallicity of the outer disc is not zero, but ∼–0.6 dex. In practice, we started computing the chemical track at 14 Gyr as before, but we introduced the dilution at 10 Gyr by hand, see Fig. 9. The derivation of the SFH is made on the [Si/Fe]-age distribution of outer disc stars, as defined in Sect. 3.2. The dilution has very little consequence on the derivation of the SFH for stars younger than 10 Gyr. The only difference is the fact that we used stellar yields at metallicities ∼0.4 dex lower than for the thick disc at the same age. This makes the system more silicon rich even for the same SFH, and the [Si/Fe]-age sequence is, therefore, naturally higher than for the inner disc. This upper [Si/Fe]-age sequence was pointed out in Haywood et al. (2013) and is shown to arise naturally as a result of the metallicity dependence of stellar yields.

The results of the fitting procedure are shown in Fig. 9. The figure also shows the chemical tracks for the dilution model, using the SFH that was derived for the inner disc. This shows an evolution very similar to the SFH fitted to the outer disc stars alone. The recovered SFR of the outer disc is very similar to that

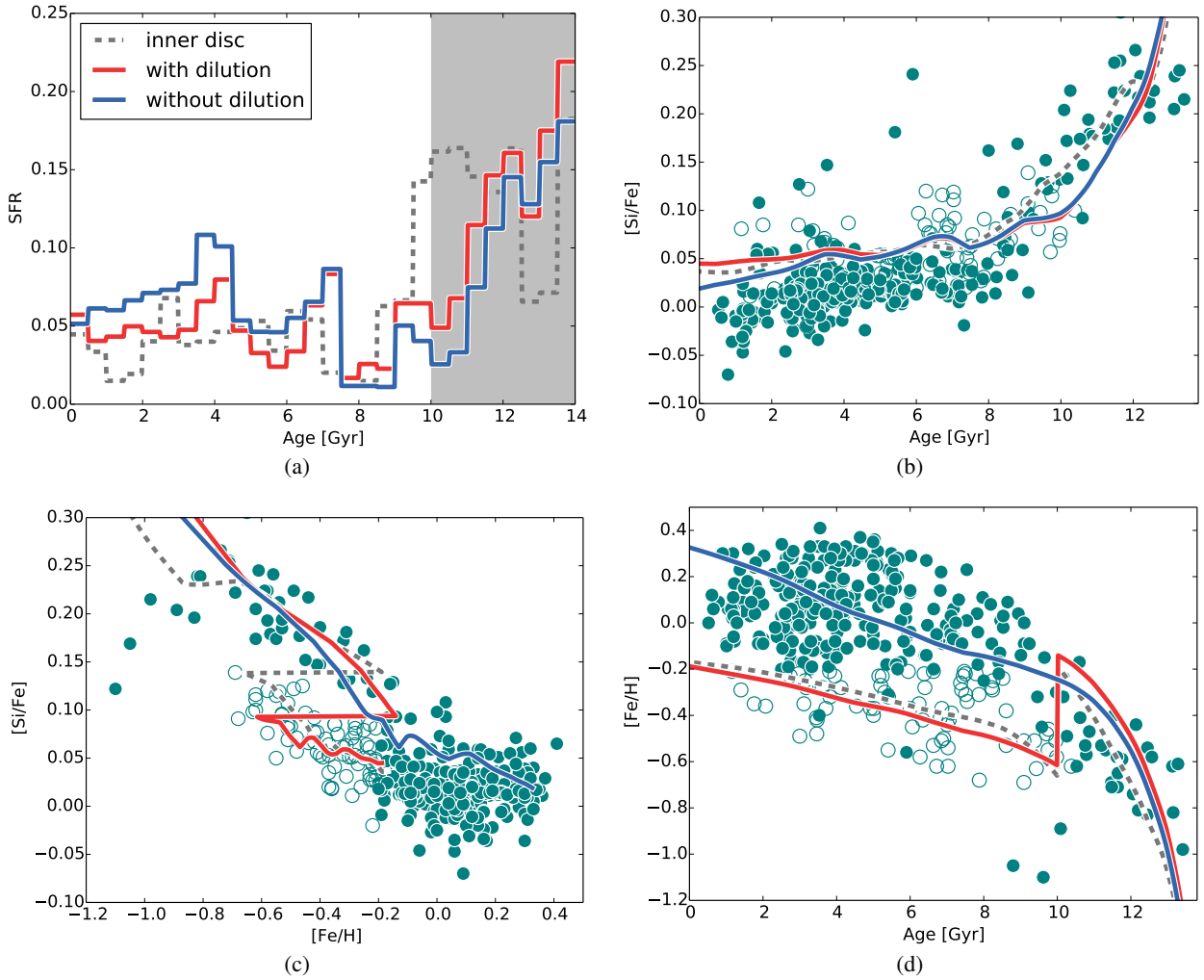

Fig. 9. Chemical evolution of the best-fit SFH to the outer disc, using silicon and the meteoric solar abundances from Anders & Grevesse (1989). The blue line is the best fit to the outer disc stars using the standard model, while the red line is the chemical track where the amount of hydrogen in the ISM is increased by 3 (the dilution model). The grey line is for the best-fit line from the inner stars (Fig. 7) using the dilution model. The grey region in panel **a)** depicts the ages before the *outer disc* begins to form and is, therefore, essentially unconstrained. All three curves are the results of the mean of the bootstrapping method used in the previous subsection. Panels **b)**–**d)** are the [Si/Fe]-age, [Si/Fe]-metallicity and metallicity-age tracks of the model and the corresponding data. The outer disc data are given as empty circles, while the inner disc is shown as filled circles.

of the inner disc in the last 10 Gyr, suggesting that, within the errors, *the inner and outer discs had similar relative SFHs.*

We also fitted the SFH calculated using outer disc stars without dilution, and it was immediately clear that without dilution it is impossible to simultaneously fit age-[Fe/H], age-[Si/Fe] and metallicity-[Fe/H].

Finally, another word on the dip. The dip in the SFH of the inner disc is generated by the change of slope in the [Si/Fe]-Age plane, it should not appear in the SFH of outer disc stars, which do not show any change of slope.

However, shortly after transition, several data points appear to have slightly higher [Si/Fe] values than the local average, which forces the fitting procedure to quickly reinitialise star formation. Whether this is real or due to the sampling of the data set awaits future studies.

6. How robust are the results?

In the following section we examine the robustness of the results presented in the previous section, following a multi-step approach.

Firstly, we discuss whether the various features in the derived SFH are robust by altering the recovered SFH. We then test how each of these adjustments changes the chemical evolution track. Secondly, because of the numerous uncertainties in the input physics of any GCE model (see, for example, François et al. 2004; Romano et al. 2005, 2010; Matteucci et al. 2009), we explore how varying the choices made when designing the basic model used in Sects. 4 and 5 (summarised in Table 2) changes the evolution of the chemical tracks. We recalculate the SFH that best fits the data when these parameters are modified. We limit our analysis and discussion to the inner disc because the results are valid for the outer Galactic regions as well.

6.1. Features of the derived SFH

In the previous section we derived the "best" SFH for the data presented in Haywood et al. (2013). In Fig. 10 we show the result of six arbitrary alterations to the best-fit SFH for the inner thin and thick disc stars. We demonstrate how certain key features in the SFH affect the chemical history of the model (see

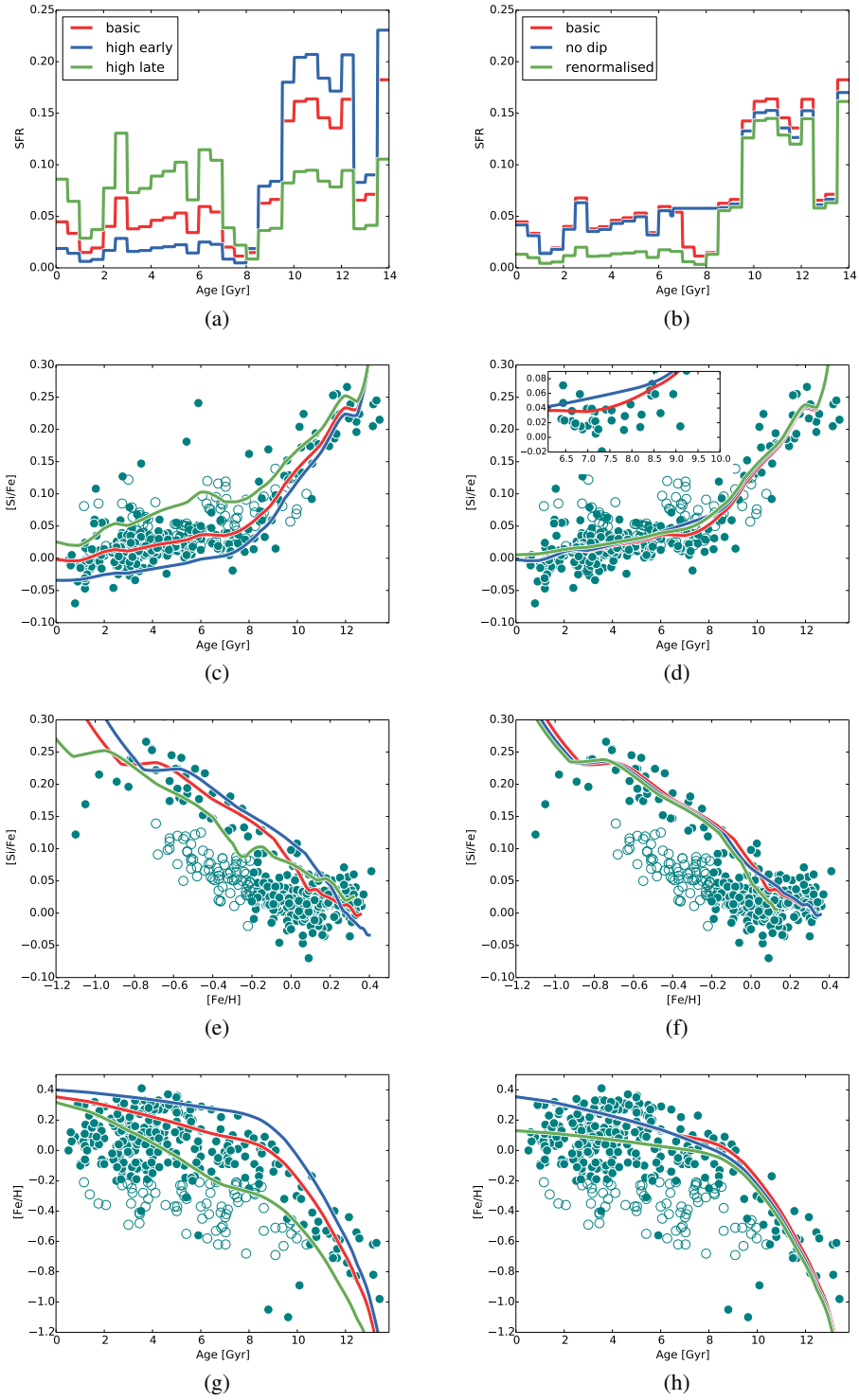

Fig. 10. Effect of alterations to the best-fit SFH on the chemical evolution of the model. Panels **a)** and **b)** illustrate the modifications to the SFR from Fig. 7. The subsequent rows are the age-[Si/Fe], [Fe/H]-[Si/Fe] and age-[Fe/H] projections. The particular case of the green SFH in the right-hand column is what happens if we reduce the SFH normalisation (A in Eq. (13)) to 0.7. The blue line is the SFH without the dip at 8 Gyr. In all plots the red line is the best-fit SFH found for the inner disc stars (from Fig. 7). The outer disc data are given as empty circles, while the inner disc is shown as filled circles. The *inset* in panel **d)** emphasizes the effect of removing the dip (green line) from the SFH compared to the basic SFH (blue line) and only shows the inner disc data.

panels a and b). This analysis allows us to better understand how the chemical evolution constrains the recovered SFH.

The left-hand column of Fig. 10 clearly shows that the [Si/Fe]-age slope constrains the early-time SFR. In panels c, e, and g, we show the results of changing the relative contributions of the star formation on each side of the dip at 8 Gyr. Where the early SFR is too high, an *excess* of iron is quickly produced, while when the early SFR is too low, *insufficient* iron enriches the ISM (panels c and g). Furthermore, panel g illustrates that the thick-disc data sets a lower limit on the early-time SFR. This is because the [Fe/H]-age track is below the thick-disc data for the low early-SFR run and above the data for the high early-SFR. Panel c demonstrates that this variation in iron is stronger than the variation in silicon because there is more silicon for a given amount of iron where the early SFR is high. Furthermore, the high late-time SFR produces a greater contrast on each side of the dip, effectively emphasizing this feature. Thus, we can see a lurch in the [Si/Fe]-age track. This allows us to gain an at least qualitative limit on the size of the dip. Finally, panel e demonstrates that despite considerable differences in [Fe/H] and [Si/Fe] with time, the [Si/Fe]-[Fe/H] tracks are not greatly dissimilar, and all overlap the thick-disc sequence. The high early-SFR

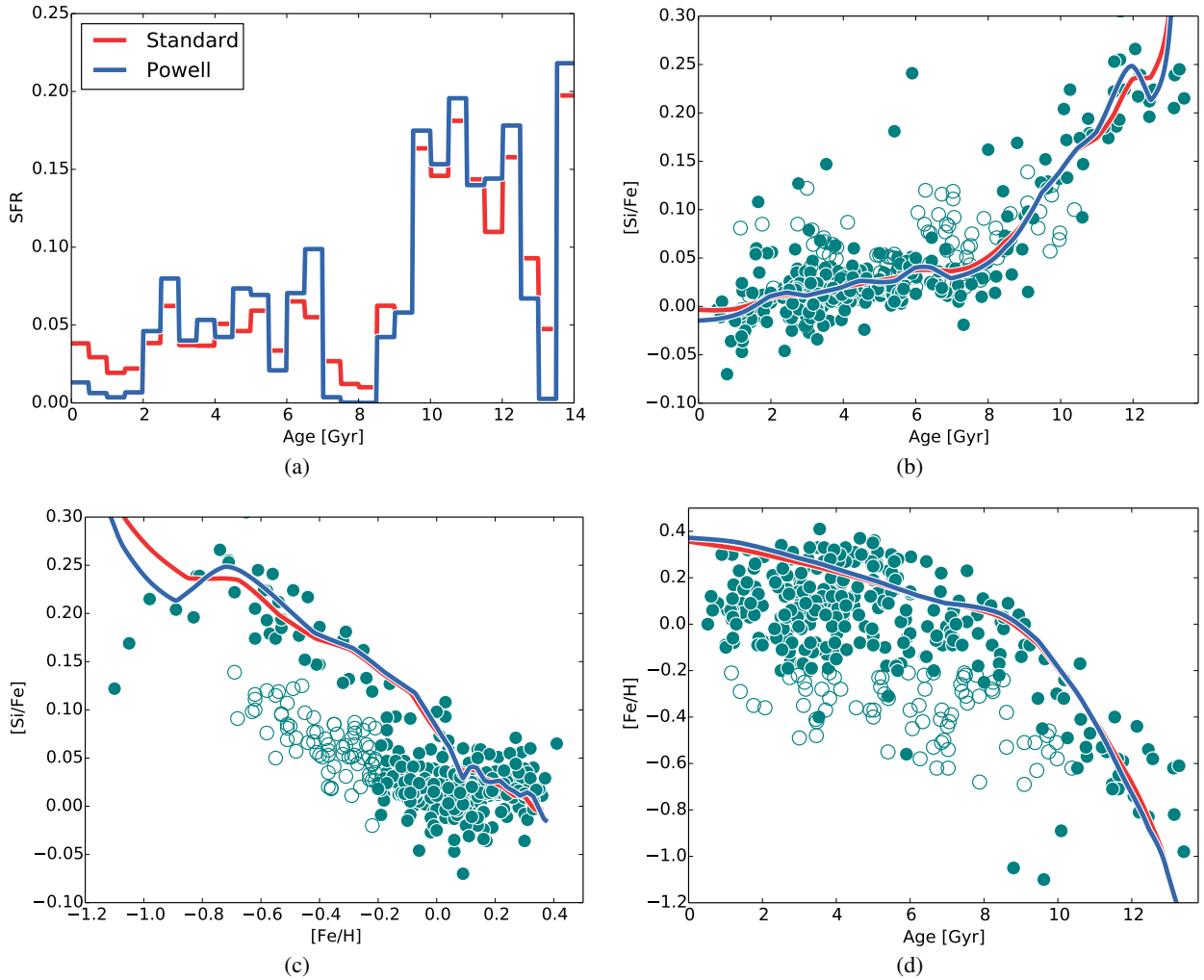

Fig. 11. Comparison between the best-fitting procedure for the standard fitting algorithm and the Powell algorithm for inner disc stars (solid circles). The outer disc stars are open circles and are given for reference.

produces more iron for a given value of [Si/Fe], suggesting that the evolution of iron is more sensitive to the relative contributions of the thick and thin discs than the silicon evolution.

In the right-hand column of Fig. 10 we present two further modifications of the SFH, which appear almost degenerate with the basic form in the age-[Si/Fe] track in panel d. The sharp transition from steep thick-disc [Si/Fe]-age slope to shallow thin-disc slope illustrates the need for the hiatus at around 8 Gyr. When we remove the dip from the SFH, the transition between slopes is more gradual and occurs at higher [Si/Fe]. The SFH is constrained by the need for this sharp transition, the location of the transition, and the size of the dip. The location of the dip is set by the transition, from steep to shallow slopes, the depth of the dip is set by the need for a sharp transition.

It might be argued that the basic chemical evolution track in panel d with the dip is still high (see the inset for a zoomed in view). The need for a potentially larger dip could be satisfied by a wider dip, as opposed to a deeper one, but this is not recovered by our fitting procedure. If there were a smaller gas fraction, for example, as a result of outflows, there would be a lower dilution of iron ejected from the SNIa. This would then emphasize that feature in the SFH, but would require us to "open the box" and allow gas inflows. This in turn would change the entire SFH, because if there is less gas present to enrich with metals, then there must be less star formation to achieve the same level of enrichment.

If we maintain our closed-box model, a complete hiatus in star formation might be required to match the data. Figure 11 shows a deeper dip and a sharper fall in [Si/Fe] at the time of the dip. This uses an alternative fitting algorithm and essentially halts star formation for ~0.5 Gyr. The resulting drop is larger and a slightly better fit to the data. Thus, these observational data show that the dip is required and robust.

Figure 11 is the result of using our fitting procedure with a different fitting algorithm. It was derived by means of Powell's method (Powell 1964), while the other fits in the paper use a Nelder-Mead simplex algorithm (Nelder & Mead 1965). The figure shows that the choice of algorithm makes little apparent difference to the recovered SFH.

We also repeated the high-early-time SFH, but reduced the total mass of stars formed over the whole time evolution to 0.7 instead of 1. The resulting chemical track (Fig. 10) fits the data points well and leaves the total mass of stars formed relatively unconstrained by the data. The recovered SFH (panel b) does, however, give a very similar thick-disc SFH to the canonical SFH, with the principle difference being in the thin disc. Here, the thick disc is very much the dominant galactic component. Panel d shows that this lower normalised curve does not produce a dip and fits the data less well at the transition

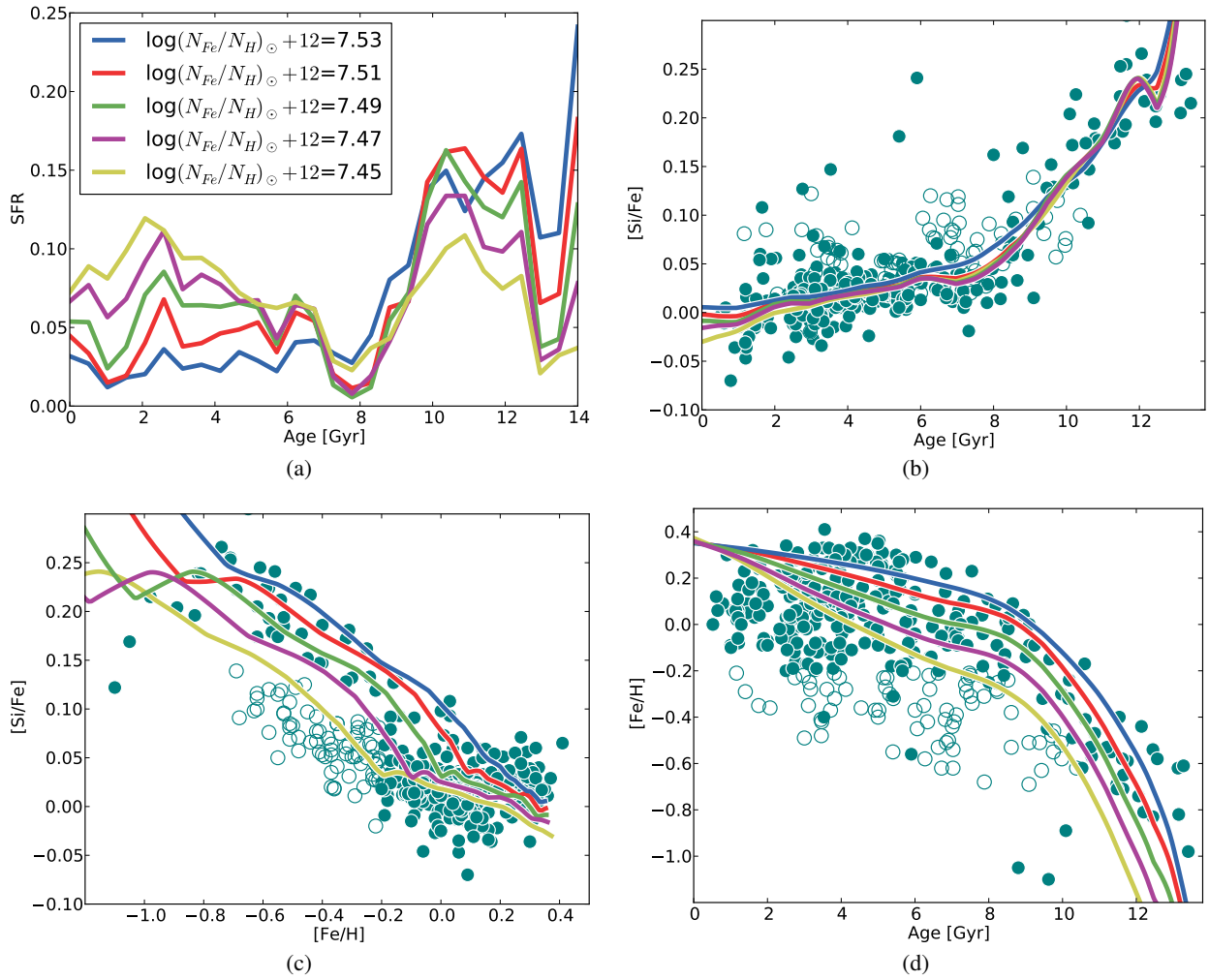

Fig. 12. Impact of changing the solar abundance normalisation on the recovered SFH (values given in the legend in panel **a**)). The different SFHs give a thick-disc mass fraction of 78%, 68%, 59%, and 48% and 39%, respectively. The red line is the mean SFH recovered in Fig. 7. The outer disc data are given as empty circles, the inner disc is shown as filled circles.

between the thick and inner thin discs. This means that this reduced SFH is less favoured than the canonical SFH. The dip cannot be resolved in this SFH because of the very low late time SFR. Another problem with this reduced SFH is that we do not produce the highest metallicity stars (panels f and h). While this SFH is, perhaps, a better fit to the centre of the [Fe/H]-age distribution, it cannot recover stars with a metallicity greater than 0.2 dex. Thus, the normalisation value must be greater than 0.7 to produce these stars.

This has implications for the origin of these stars. The model with the standard normalisation can fit these metal-rich stars, but if the normalisation is not equal to unity then the super-solar-metallicity stars must come from the inner regions of the galaxy. The effect of the normalisation is discussed below in greater depth.

This figure clearly shows that the late-time SFH is more poorly constrained than at early times. The late-time chemical tracks can be made to follow the data for a range of changes to the SFH. The divergences from the data and the basic SFH tracks appear mainly because of changes to the SFR at early times. However, the requirement for a sharp transition from the steep [Si/Fe] slope at early times to a shallower slope at later times means that we require the existence of the dip. For the dip to appear, there needs to be sufficient contrast between the trough of the dip and the SFR on either side.

6.2. Solar values

The fitting procedure is extremely sensitive to the chosen solar abundance offsets. Our best-fitting procedure fails to match the age-[Si/Fe] and the metallicity-[Si/Fe] distributions concurrently when the solar abundances are changed by too much. The reason why the model is so sensitive to the solar values is best illustrated in Fig. 5, particularly panel b. The narrow range (about 0.05 dex) of possible final values for the [Si/Fe] means that a small shift in the solar abundance normalisations can move the chemical tracks to regions of the parameter space where a good fit to the data is impossible. For example, the run where the solar iron is 7.45 lies off the thick-disc sequence in panel c.

We used our best-fitting procedure to recalculate the SFH using different solar normalisations (Fig. 12). We altered the solar iron abundance because this value differs between the standard Anders & Grevesse (1989) that we prefer and the value used for iron in the data from Adibekyan et al. (2012).

There is a distinct change in the form of the recovered SFH with changing $A(\mathrm{Fe/H})_\odot$, shown in Fig. 12. Here, $A(\mathrm{Fe/H})_\odot$

indicates the value of $\log(N_{Fe}/N_H) + 12$ in the sun. Lower $A(Fe/H)_\odot$ values require a lower early-time SFR and higher late-time SFR than the SFH recovered for high $A(Fe/H)_\odot$ values. Indeed, the fraction of stars in the thick-disc part of the distribution (ages > 8 Gyr) ranges from 78% to 39% for $A(Fe/H)_\odot$ = 7.53, 7.45, respectively, which is a considerable difference for a solar abundance change of only 0.08 dex (which corresponds to a change of 20%).

The metallicity-[Si/Fe] data (panel c) is best fit by the intermediate range, that is, 7.49−7.53; with the best fit to this plot would be 7.51, the value from Anders & Grevesse (1989) used before.

It is crucial to point out that even for $A(Fe/H)_\odot$ = 7.47 (the value used for the data from Adibekyan et al. (2012)) over half the mass is in stars with ages greater than 8 Gyr. As previously discussed, we used the Anders & Grevesse (1989) value for our solar iron normalisation, *not the one used for the data*, to more accurately fit the [Si/Fe]-[Fe/H] distribution.

Without changing the solar abundance of iron from the value of 7.47 used in Adibekyan et al. (2012) to the Anders & Grevesse (1989) value of 7.51, the track passes through the lower end of the thick-disc envelope in the metallicity-[Si/Fe] plot and not through the centre.

The results remain qualitatively the same whether we employ the solar normalisations used in the data or our preferred value from Anders & Grevesse (1989). Even when the mass of the thick disc was slightly reduced, it retains a mass similar to that of the thin disc. This is justified by the uncertainties in the yields and the lack of consensus on which set of theoretical yields accurately reflect the observations. If the stars in the yield tables produce slightly less iron, for example, it will have the same effect as a high $A(Fe/H)_\odot$. There is also no accord in the literature as to the abundance of elements in the sun, such that even recent solar values (e.g. Asplund et al. 2009) are not universally adopted (e.g. Adibekyan et al. 2012).

It is interesting that a shift of only 0.02 dex can result in considerable changes in the track in panels c and d. It can be seen that amplifications of up to four or five times the offset in the solar value occur. Owing to the narrow range in final [Si/Fe] value discussed earlier, the SFR must change considerably with changing solar iron value to fit to panel b. This has a much more significant effect on the total amount of metals ejected at any given time than on the abundance ratios. The total metallicity is more sensitive to the SFH than is the [Si/Fe] evolution, as can be seen in Fig. 5.

It is also worth noting that the spread in end-point metallicity is smaller than in the offset in solar iron value. The end-point values vary from 0.350 to 0.373 for the $A(Fe/H)+12$ values of 7.53 and 7.45. This is because there is more iron locked up in stars that have not yet produced an SNIa in the low solar iron case than in the high solar iron case because of the form of the recovered SFH. The actual value of the solar iron normalisation effectively compensates for this locked-up fraction.

It is telling, however, that the transition time from the thick disc to the thin disc does not change considerably, and that, except for the extremely high solar iron value, the dip is clearly visible. It is noted, however, that where the dip does occur, it is always in the same place, irrespective of solar value. The knee feature still appears robust.

6.3. IMF variations

An important consideration in a chemical evolution model is the effect of the IMF. The functional form of the IMF controls the fraction of stars with a particular mass that forms from a given amount of gas. This has important consequences for the chemical evolution because the amount of a given metal released when a star dies depends on the mass of that star. There is a considerable history of IMFs beginning with Salpeter (1955) and continuing to the present day. Furthermore, because the IMF must be normalised, and some IMFs, such as the Salpeter (1955) IMF, are divergent, a suitable range of masses must be chosen over which to integrate. For each IMF we explored, we normalised the function by integrating between a mass of 0.1 and 100, as is traditional. We selected a range of common IMFs from the literature and implemented them in our model.

We show in Fig. 13 how various IMFs affect the chemical tracks while keeping the same SFH. By using the same SFH, we can explore how the different IMFs change the contributions of silicon, iron and the amount of gas released, in a controlled way. We chose the often used IMFs of Salpeter (1955) and Kroupa (2001), the historically important Scalo (1998) IMF, and for illustrative purposes, the IMF of Baldry & Glazebrook (2003). These are representative of the range of IMF gradients that have been proposed, and are useful to compare with other work.

The functional form of our chosen IMFs is summarised in Table 3. We see some interesting behaviour in the IMFs, in that the different panels of Fig. 13 provide different details. The simplest form is the old Salpeter IMF, which has no change in slope, while the Kroupa IMF has a similar slope (−1.3 compared to −1.35), but a break at one solar mass. The Baldry IMF has a shallower slope, meaning proportionally more high-mass stars, while the Scalo IMF has a steeper slope, meaning proportionally fewer high-mass stars.

Figure 13 shows that, as expected, the Kroupa and Salpeter IMFs produce similar chemical tracks, although the Kroupa IMF is slightly more iron abundant than the Salpeter IMF. This is due to the break in the IMF at 1 $M_\odot$. SNIa and AGB stars involve a component of the IMF where $M < 1\ M_\odot$, which occurs at later times but mainly because it also changes the normalisation of the IMF, which is calculated by the integral of the IMF between 0.1 and 100 solar masses. Panel b, however, shows that for a given metallicity, the Kroupa IMF has more silicon than the Salpeter IMF. This is also a result of the shape of the IMF, which produces more high-mass stars in the Kroupa IMF because of the (slightly) shallower slope.

Table 3. Various IMFs taken from the literature as defined in Table 2 of Baldry & Glazebrook (2003).

Name	0.1−0.5	0.5−1.0	1.0−10.	10.−120	C
Kr01	−0.8	−1.7	‖		0.331
S55		−1.35			0.171
Sc98	−0.2		−1.7	−1.3	0.395
B03	−0.5		−1.2		0.323
SSP mass fraction					
Name	SNII	AGB	8−3.	2.6−1.8	1.5−0.9
Kr01	0.363	0.630	0.233	0.111	0.187
S55	0.337	0.655	0.235	0.117	0.202
Sc98	0.240	0.750	0.207	0.135	0.286
B03	0.792	0.207	0.121	0.030	0.030

Notes. IMFs are normalised between 0.1−100 $M_\odot$. Kr01 is from Kroupa (2001), S55 is Salpeter (1955), Sc98 is from Scalo (1998), B03 is from Baldry & Glazebrook (2003). C is the constant of normalisation between 0.1 and 100 $M_\odot$. The lower section of the table shows the integrated mass fraction of stars involved in SNII, AGB, and the different components of the SNIa.

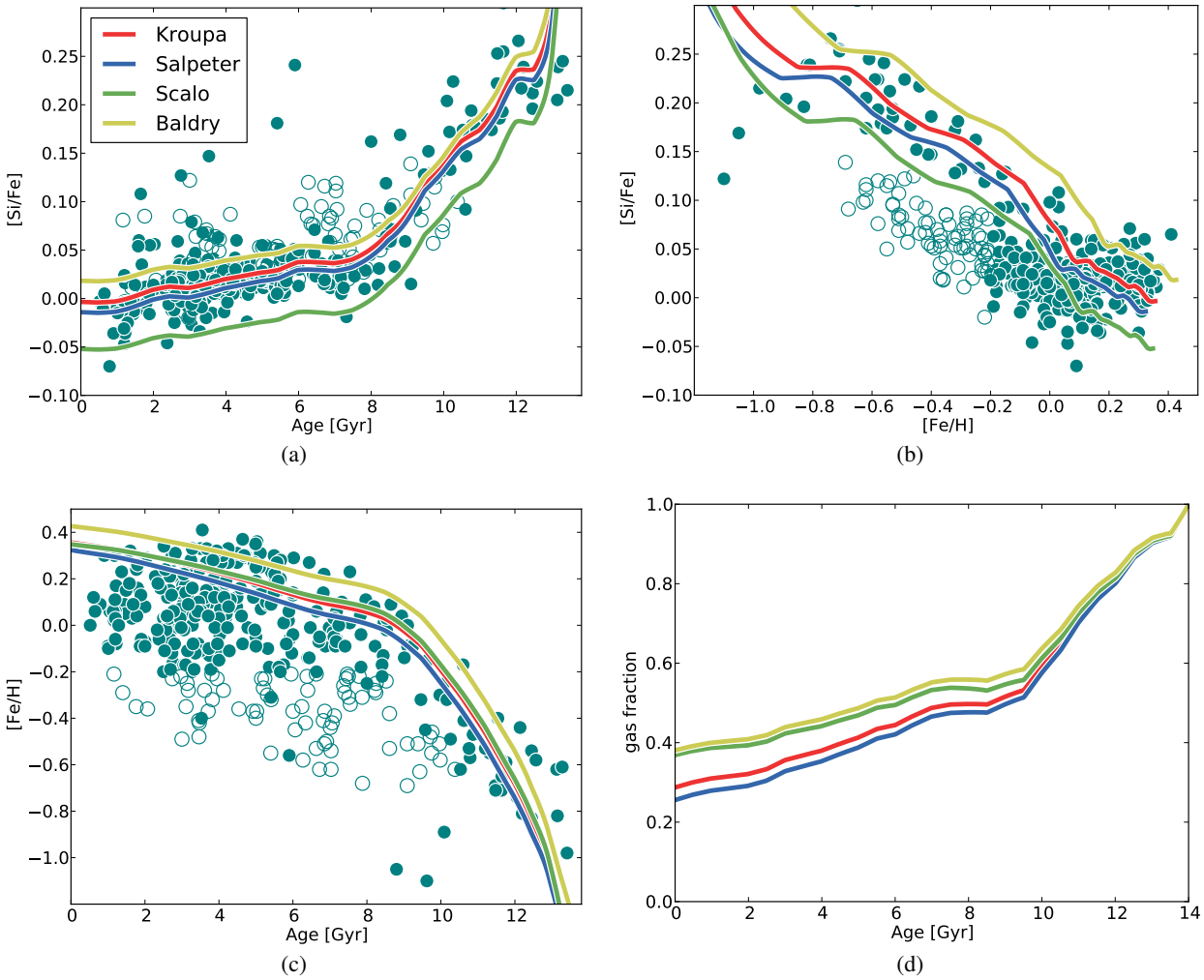

Fig. 13. Chemical tracks using different IMFs (shown in Table 3) using the SFH derived from fitting the inner disc stars in Sect. 5 (Fig. 7, panel **a**)). Only the IMFs are changed, the SFH is the same in each run. The chosen IMFs are given in the legend in panel **a**). Panel **a)** shows the evolution of [Si/Fe] with stellar age. Panel **b)** shows the evolution of [Si/Fe] with metallicity, panel **c)** shows the evolution of metallicity with age, and panel **d)** shows the evolution of the gas fraction. The points are data from Haywood et al. (2013) and open circles depict outer thin disc stars, while solid circles are thick-disc and inner thin-disc stars.

Panel a shows that the [Si/Fe]-age evolution of the Kroupa and Salpeter IMFs are almost identical, while the Scalo IMF is the less iron abundant relative to the silicon and is more different to the data than the other IMFs. The end-time difference of the [Si/Fe] of each IMF from the standard Kroupa IMF (used hitherto) is −0.01, −0.05, and +0.02 for the Salpeter, Scalo, and Baldry IMFs, respectively. The end-point metallicity differences are −0.03, −0.006, and 0.07 at age = 0, but with a maximum difference of 0.07, 0.05, and −0.17, respectively. The Kroupa, Scalo, and Salpeter IMFs give fairly similar metallicity tracks with a much more divergent Baldry IMF.

The explanation for these differences are the shape of the IMFs and the mass fraction of the stellar population that releases gas.

1. The Baldry IMF produces more SNII than SNIa, and so the ISM is more silicon rich while producing more gas overall (panel d). The ISM is, therefore, enriched more than in the other IMFs. This is why the Baldry IMF track is the rightmost track in panel b.
2. A considerable fraction of the iron is made in SNIa and is lacking in the Baldry IMF (compared to the Kroupa IMF) because of the shallower slope. The vast (relative) overabundance of SNII means, however, that overall, the Baldry IMF produces more iron than the other models. This high level of SNII is also why the gas fraction is higher.
3. For the Scalo IMF, the lack of SNII relative to the Baldry IMF is compensated for by the higher proportion of low-mass stars (and SNIa and AGB stars). This means that the gas is returned to the ISM more gradually and explains the lack of [Si/Fe] in panels b and a, that is, the iron has not yet been returned to the ISM.
4. The Salpeter IMF produces the least gas because of the higher proportion of stars with $M < 0.9\ M_{\odot}$ that have not yet released their gas and metals.

Other popular IMFs are not shown because of the similarity between them and either the Salpeter or Kroupa IMFs. The popular Chabrier (Chabrier 2003) IMF, for example, has a slope identical to the Salpeter IMF but a locked-in fraction (stars that have not yet ended their lives) similar to the Kroupa IMF.

Figure 14 shows the different SFHs (panel a) and chemical tracks recovered by using the bootstrap procedure on each of the four selected IMFs. We once again attempted to fit the inner thin and thick discs. Each IMF can be closely fit to the age-[Si/Fe] distribution (panel b), but shows markedly different

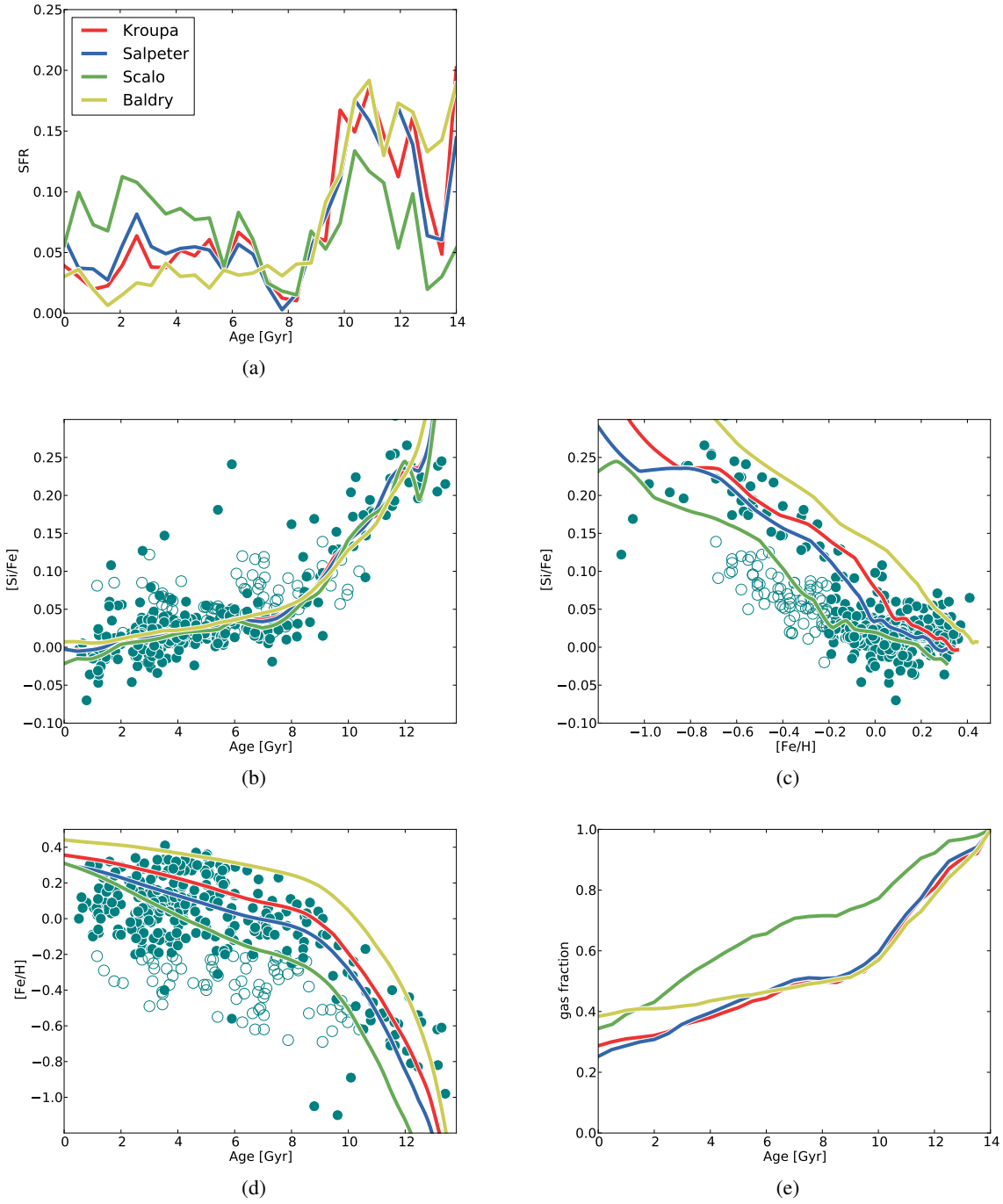

Fig. 14. Chemical tracks of the best-fit SFHs using the different IMFs described in Table 3. The chosen IMFs are given in the legend in panel **a)**. Panel **a)** shows the different fitted SFHs, panel **b)** shows the evolution of [Si/Fe] with stellar age and is the distribution used to fit the data. Panel **c)** shows the evolution of [Si/Fe] with metallicity, panel **d)** shows the metallicity evolution with stellar age, and panel **e)** shows the evolution of the gas fraction with time. The points are adapted from Haywood et al. (2013). Open circles are outer thin-disc stars, solid circles are thick-disc and inner thin-disc stars.

tracks through the metallicity-[Si/Fe] and age-metallicity distributions. The Baldry IMF overproduces iron, while the Scalo IMF is under-abundant in iron. The Kroupa and Salpeter IMFs are fairly similar. This suggests that we should discard the Scalo and Baldry IMFs based on these data. The different IMFs also imply a different fraction of stars in the thick disc, ranging from 37% (Scalo) to 61% (Baldry). There is considerable degeneracy between varying the solar abundance and choosing the IMF. Moreover, the SFH derived for the Scalo IMF produces a much more gas-rich ISM (panel e), and the Baldry IMF does not recover the dip at 8 Gyr.

6.4. Normalisation

At this point, it is useful to discuss our choice of normalisation, A. In the rest of the paper we have required that the integral of the SFH is equal to unity. Essentially, this sets the star formation

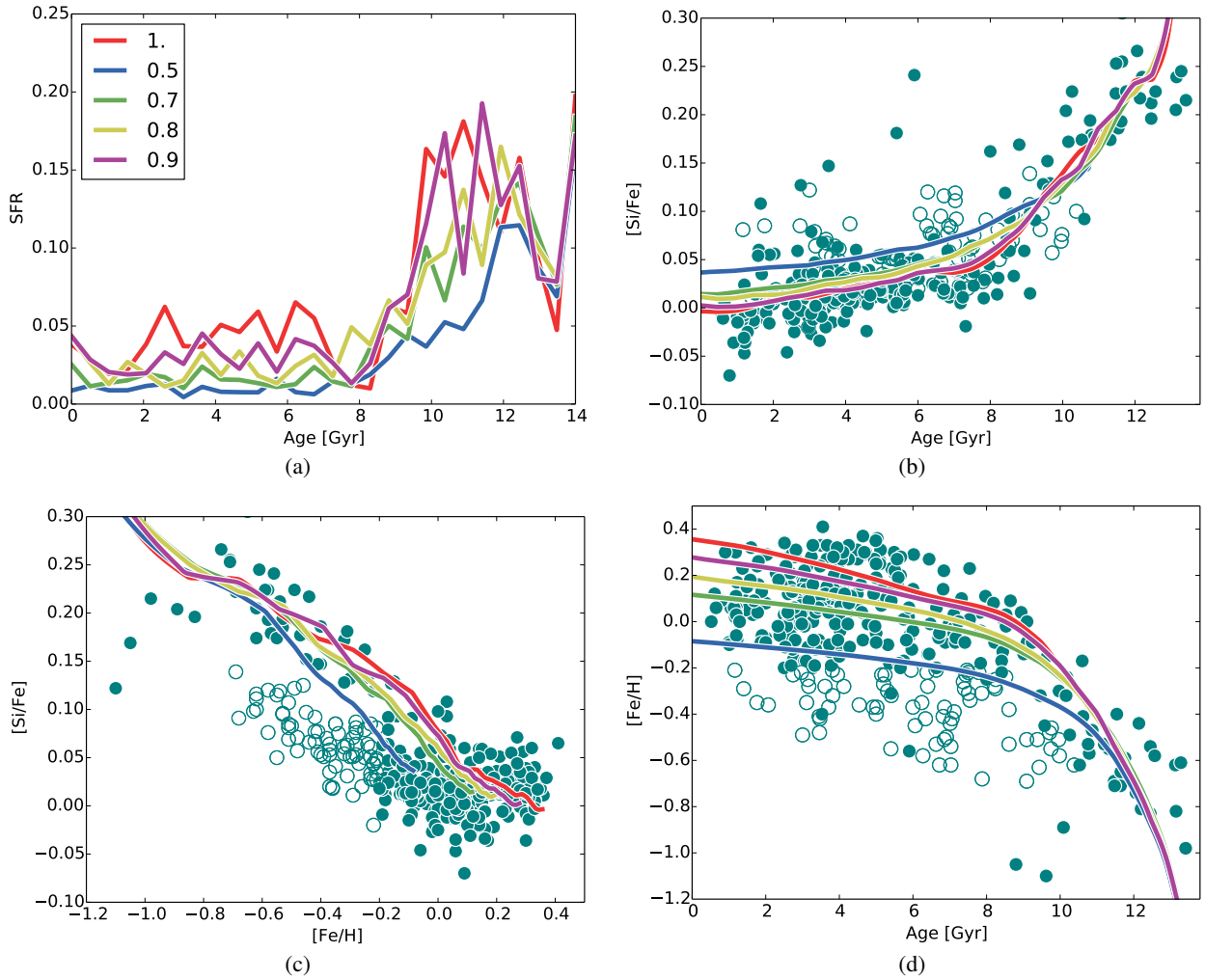

Fig. 15. Comparison between the best-fit (to thick- and inner thin-disc stars) chemical tracks for different total SFH normalisations. The values of the integral of the SFHs are given in the legend in panel **a)**. Panel **a)** shows the different fitted SFHs, panel **b)** shows the evolution of [Si/Fe] with stellar age and is the distribution used to fit the data. Panel **c)** shows the evolution of [Si/Fe] with metallicity, and panel **d)** shows the metallicity evolution with stellar age. The points are adapted from Haywood et al. (2013). Open circles are outer thin-disc stars, solid circles are thick-disc and inner thin-disc stars.

efficiency of the system, with lower values having less efficient star formation.

The first clear result of lowering A is that it quickly destroys the otherwise robust dip feature (Fig. 15). Although at $A = 0.5$ the age-[Si/Fe] track does not evolve to an iron-rich enough end state, where at $A > 0.7$ the chemical tracks match the data fairly well because of the intrinsic scatter. Nevertheless, it is only in the normalisation equals 1 case that the dip and knee are very sharp (panel b).

One potential advantage of these lower ($A > 0.7$) normalisations is that they have a low [Fe/H] end state and so identify high metallicity stars that are assumed to originate from subsolar Galactic radii (as suggested in Sect. 6.1).

One would naively assume that changing A would have only a minimal impact on the chemical evolution, other than to shift the plot to lower [Fe/H] values. However, this simplistic view is complicated by the fact that the yields from stars depend on the metallicity at which the star is formed. This is why introducing a dilution changes the track in [Si/Fe] in the outer disc. The physical interpretation of the normalisation is simply that the ISM is more massive than the stellar mass of the galaxy, and so ejected metals are diluted into a greater quantity of primordial gas. Thus, the star formation efficiency is less intense.

A further impact of lowering the normalisation is that there is insufficient contrast between the top and bottom of the dip at 8 Gyr, and so this feature no longer has an effect on the chemical evolution.

6.5. Using different elements

Here we discuss the differences in the tracks of magnesium and oxygen using SNII yields from Nomoto et al. (2006) and SNIa yields from Iwamoto et al. (1999). We chose to follow these elements in addition to silicon because magnesium is also used in Haywood et al. (2013), and oxygen is both the dominant α-element and very common in numerical simulations (e.g. Brook et al. 2012; Gibson et al. 2013). These elements differ from silicon because they are produced in high amounts by SNII alone, while silicon has contributions from both types of SN. We used the Anders & Grevesse (1989) solar normalisation for magnesium and the solar normalisations derived by Ramírez et al. (2013) for oxygen and iron when dealing

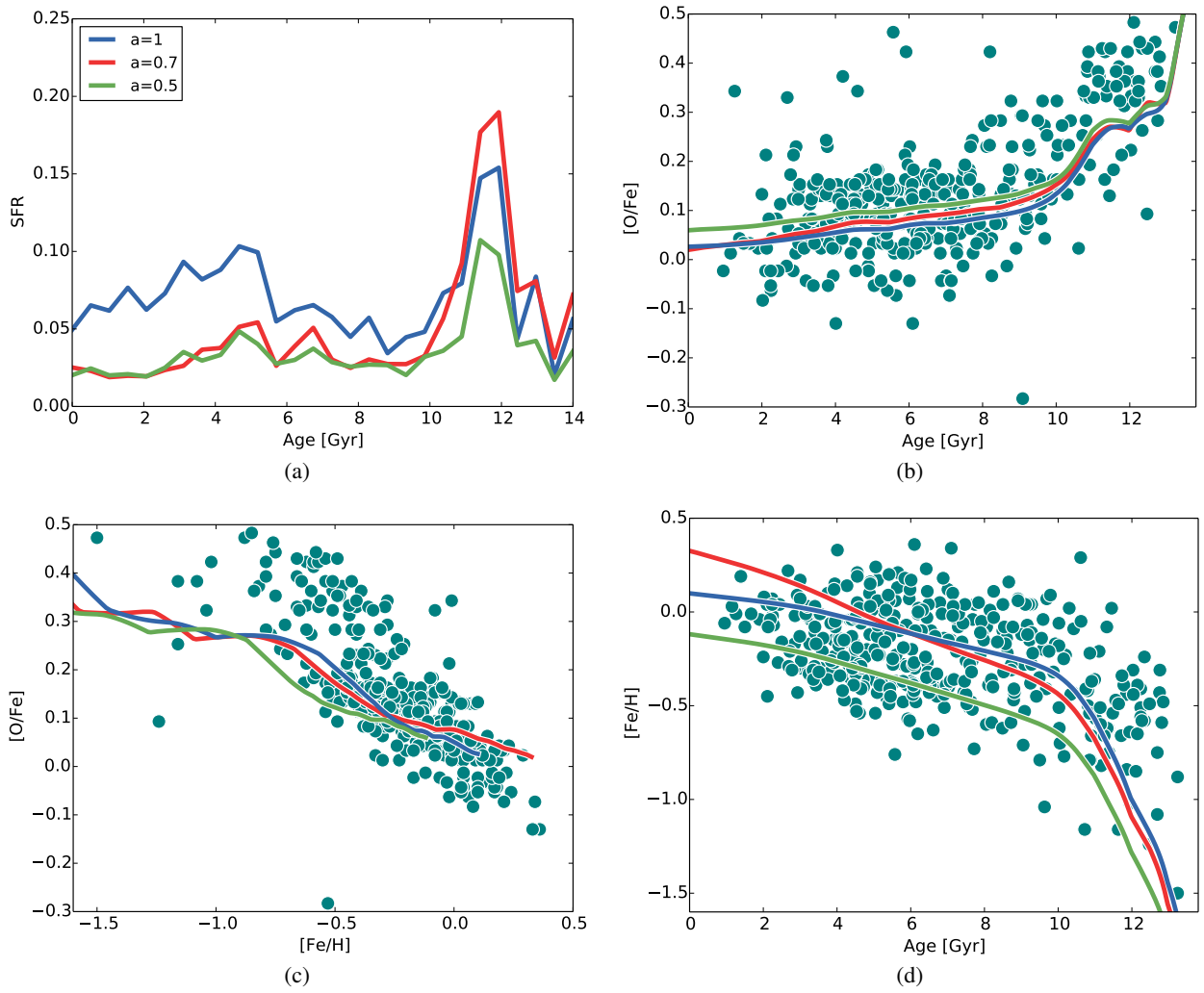

Fig. 16. Best-fit SFR for oxygen abundances for different total normalisations of the SFH. The values used in the normalisation are given in the legend in panel **a)**. The points are Ramírez et al. (2013) data.

with oxygen data[4]. We discuss the oxygen tracks and data first and then explore the differences between the three different α species.

The best-fit SFH for oxygen has a significantly different form (Fig. 16, panel a). There is a low initial SFR, which is needed so that the [O/Fe] track is close to the thick-disc sequence in panel b. Even so, the oxygen track lies below the thick-disc data. This low initial SFR has an impact on the initial rise of the [Fe/H]-age track (panel c). The initial rise in [Fe/H] is slower than the data suggest, and so does not reach the [Fe/H] values of the oldest stars. The low initial SFR is followed by a peak in SFR for each of the three normalisation values. The ratio of the early-to-late time SFR is lowest for the case where $A = 1$ (where A is the normalisation), but has a similar form to the SFH recovered for silicon where A <1. However, there is no dip at 8 Gyr in any of the oxygen SFHs. This may be due to either the solar normalisation (discussed in the previous subsection) or the larger scatter in the dataset.

Figure 16 shows the best-fit SFH for the oxygen yields and ages from Ramírez et al. (2013). There is considerably more scatter in the data in the age-[O/Fe] plot than in the sample of Haywood et al. (2013), and it was not possible to identify a specific inner and outer disc using oxygen abundances. This is because the data from Ramírez et al. (2013) have a significantly lower signal-to-noise ratio than the data from Adibekyan et al. (2012). The best-fit SFHs give a poor fit to the metallicity-[O/Fe] distribution in panel c and shift the tracks to the lower left hand side of the plot. If we assume that the yields from Nomoto et al. (2006), Karakas (2010) and Iwamoto et al. (1999) and our tracks for SSPs (Sect. 2.2) are correct, then these plots suggest that there has been considerable dilution of the metals due to either gas inflow or some other process. Considering the uncertainties in the theoretical yields and the choices we have made in our model, however, it is impossible to know whether it is not just a matter of inaccurate theoretical stellar yields. A solution to this problem may involve a modification to our truncation of the stellar yields at 40 solar masses. This works well for silicon, but is, perhaps, less appropriate for oxygen and/or magnesium (see below). Including the yields from stars with $M_* > 40\ M_\odot$ is apparently required to produce enough oxygen to match the data, but a straight extrapolation to higher masses overestimates the amount of oxygen. This would require a much more massive thick disc to lower the [O/Fe] value to match the data, see Fig. 5.

[4] These values are given as 8.64 and 7.45 for oxygen and iron from Ramírez et al. (2013). In Anders & Grevesse (1989) the Si, Mg and Fe values are 7.55, 7.53, and 7.51, respectively.

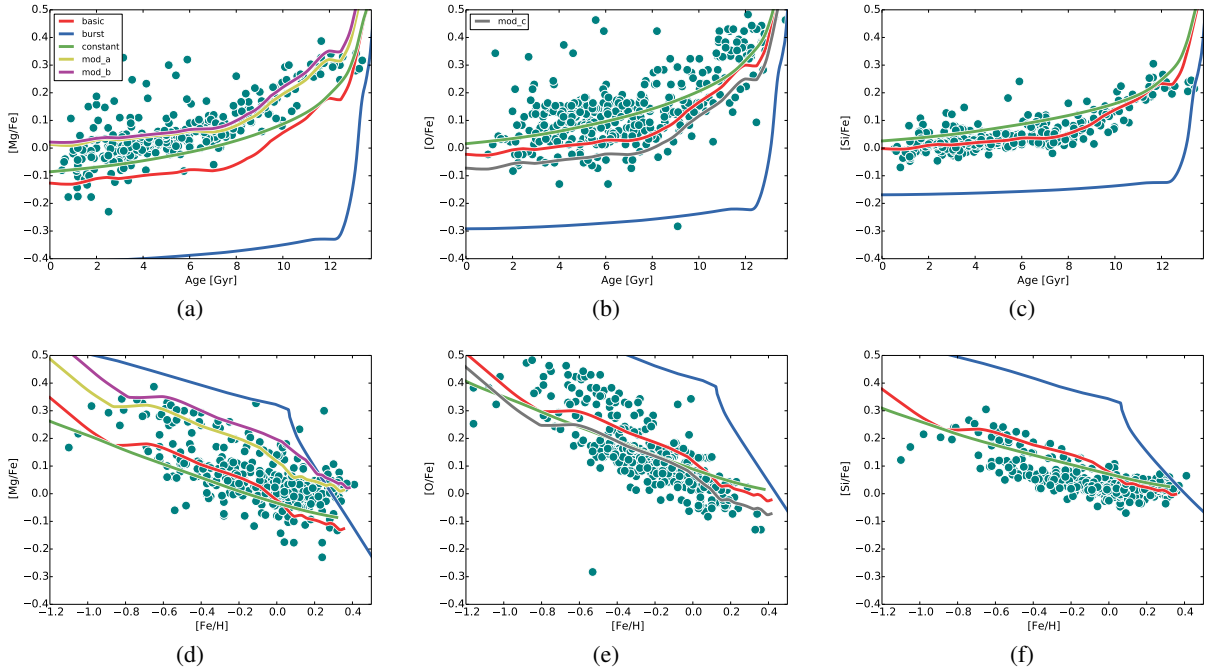

Fig. 17. Chemical evolution of [α/Fe] with age and metallicity for several SFHs. We used the best-fit SFH for silicon (Fig. 7) using meteoric solar abundances from Anders & Grevesse (1989) ("basic", red line) as well as a sharply initially bursting SFH ("burst", blue line) and a constant SFR ("constant", green line). The *left-hand column* shows the magnesium evolution, the *centre column* shows the oxygen evolution, and the *right-hand* column shows the silicon evolution. The additional lines illustrate various modifications to the best-fit SFH. "mod_a" (yellow line) is the track based on the "basic" SFH, where a constant of 0.14 dex has been added to the solar magnesium. "mod_b" (purple line) is the track where a constant of 0.18 dex has been added to the "basic" track, but the late-time (stars older than 8 Gyr) SFR has been reduced by 2. "mod_c" (grey) is the "basic" track where the solar oxygen value is shifted by −0.05 dex.

As a result of the scatter in the data, the separation between the inner and outer thin discs seen in the sample of Adibekyan et al. (2012) is not apparent (see panel c). This, as well as the uncertainties in the model, may be hiding the details of the SFH, such as the dip.

It is noticeable in the recovered SFHs that a high SFR during the thick-disc era is required, followed by a long period of lower star formation to fit the data. This is qualitatively the same as for silicon and confirms that the thick disc is a substantial component of the Galaxy, formed during an intense phase of star formation.

When we fitted the age-[O/Fe] distribution in the same manner as the age-[Si/Fe] track, we found that we could not fit the [Fe/H]-[O/Fe] plot at the same time. Additionally, using the dataset from Ramírez et al. (2013), there is no clear way of splitting the data between the thick disc/inner thin disc and the outer thick disc in the data from Haywood et al. (2013). The slope of the data in [O/Fe]-[Fe/H] is too shallow for our model to recover. The best-fit SFH also fits the [O/Fe]-age distribution fairly well if we shift it by 0.05 dex (panels b and e), except at high [Fe/H] in panel e.

The data for oxygen (see Figs. 4 and 16) show the same tightly correlated thick-disc component and a change at around 8 Gyr. *The recovered SFHs are different for silicon and oxygen, but in the details rather than in the general case.* Either way, the thick disc is very massive and contains ∼38%, ∼56%, and ∼48% of the stars for $A = 1.0$, 0.7, and 0.5, respectively. In each case this would give the thick disc a mass of around 2.1×10^{10} $M_\odot$, 3.2×10^{10} $M_\odot$, and 2.7×10^{10} $M_\odot$ assuming a total Milky Way stellar mass of 5×10^{10} $M_\odot$.

Using a selection of three simple SFHs, the oxygen and magnesium abundance tracks can be compared to the silicon tracks and the data. Our model under-produces magnesium relative to the iron to an extent of 0.14 dex or 40% (Fig. 17, panel a). The late-time slope is flatter than in the observations for this element, and the evolution of [Mg/Fe] is not bracketed by burst and constant SFHs, suggesting that, if it is to be fitted at all, the SFH would be increasing.

The [O/Fe] evolution is an equally poor match to the data as magnesium for any SFH (panels a and b Fig. 17), this is equally true in the metallicity-[α/Fe] tracks. These tracks show that the data lie between the burst and constant SFHs for magnesium and oxygen. Silicon is by far the best at fitting both the panels.

Using the model in Table 2, the magnesium evolution cannot be converged to the data. If the data are only just covered by the increasing SFR (i.e. where $y = kx$ and k is the constant of normalisation), the features of the plots cannot be recovered using our best-fit procedure. An alternative approach would be to release the requirement that the integral of the SFR is equal to one, allowing $A < 1$ and thus producing a greater variation in the end point of the age-[Mg/Fe] evolution. This influences the [Fe/H] distribution considerably, however, shifting the tracks to lower [Fe/H]. This means that the [Fe/H]-[Mg/Fe] cannot be recovered simultaneously with age-[Mg/Fe]. Alternatively, this difference could be a matter of using the correct IMF, improved yields, etc. Although we have offset the solar iron value in the last section to fit the data well, the magnesium would require a much more significant offset to fit the distribution of points.

This demonstrates that the theoretical magnesium yields do not correspond well to the observed chemical evolution of the Galaxy. This is another reason why we consider the [Si/Fe] fit most appropriate for this paper.

However, when we shifted the magnesium value so that the theoretical ratios between magnesium and silicon were the same

as in the data (a shift of +0.14 dex), we found that the early-time canonical silicon SFH reproduces the [Mg/H]-age fairly well (Fig. 17, panels a and d). At later times a reduction of 50% of the SFR improves the fit even more (with a shift to +0.18 dex). The [Fe/H]-[Mg/H] is also recovered well.

Conversely, we can interpret this more negatively. The model under-produces magnesium relative to iron to an extent of 0.14 dex or 40% (Fig. 17). (Again, a possible solution involves the extrapolation to high-mass stars, i.e. $M_* > 40$.) The late-time slope is flatter than in the observations of magnesium, and the evolution of [Mg/Fe] is not bracketed by a flat SFR. This suggests that, if it is to be fitted at all, the SFH would be *increasing with time*.

As previously discussed, there is considerable variation between the available theoretical yields, each of which return different chemical tracks for a given element. With this uncertainty in mind, it is unsurprising that for any given set of yields the various species return varying SFHs. It is encouraging that silicon, oxygen, and magnesium return SFHs that are similar.

6.6. Yields and metallicity threshold for SNeIa

The results presented in Sects. 4 and 5 are based on the adoption of yields from Nomoto et al. (2006) for SNII, the yields for AGB stars from Karakas (2010), and the yields for SNIa from Iwamoto et al. (1999). Here, we discuss the extent to which the recovered SFH of the Galaxy is sensitive to this choice, and how much the results would change if we adopted another set of yields for SNII and SNIa. This topic has been extensively studied by other authors (e.g. Romano et al. 2010), but we include it here for completeness.

We also show the impact on the SFH of adopting a metallicity threshold of $Z = 0.1\ Z_\odot$, as in Matteucci (2009) and Kawata & Gibson (2003) for the onset of SNIa. This choice is justified in the work of Kobayashi et al. (1998). The origin of this concept is that only gas with [Fe/H] > -1 can produce the optically thick winds required to stabilise gas accretion onto the white dwarf. However, more recent observations suggest that SNIa can occur very early in the history of the Universe, throwing doubt on the existence of any threshold (Mannucci et al. 2005, 2006), which is why we did not implement it in the main model used here.

Figure 18 shows the huge impact of using different SNII yields on the chemical evolution model. We chose yields from Woosley & Weaver (1995) as an alternative to those from Nomoto et al. (2006) because they are the most common in the literature. We included the modification to the yields from Woosley & Weaver (1995) by Timmes et al. (1995), however, where the iron abundance is divided by two. This is required to obtain a high enough initial [Si/Fe] value at $t = 14$ Gyr (the oldest stars). The alternative SNIa yields are taken from Travaglio et al. (2004). For all the choices adopted in this section, we ran our best-fit procedure on the inner disc stars to recover the corresponding SFH.

It is clear from Fig. 18 that the recovered SFH using the yields from Woosley & Weaver (1995) produces chemical tracks that are very poor fits to the data. We find the following:

1. The end point in the age-[Si/Fe] is too high in all cases, with the worst fit being the model where a metallicity threshold for the onset of SNIa is included (panel c).
2. The metallicity-[Si/Fe] track shows that there is too much iron for the given [Si/Fe] ratio as well (panel g).
3. The age-[Fe/H] track (panel e) shows that most of the iron forms too early.
4. The SFH for these yields all bursts very early (panel a) and has an almost exponential form.

We would expect to evolve in age-[Si/Fe] most quickly for the sharp early burst (see Sect. 4.1). This implies that there exists no possible SFH that can fit the data using these yields (in this model).

For the yields from Nomoto et al. (2006), the model with the SNIa threshold is again the poorest match of the three models employing these yields (right column, Fig. 18). Using the different SNIa yields produces tracks that are indistinguishable in either the chemical tracks or the recovered SFH, however. Thus, we do not require an SNIa metallicity threshold to fit the data, and find that such a threshold actually hinders fitting.

7. Discussion

7.1. Summary of results

We found that fitting our model to the chemical trends as a function of age is a very effective way to recover the SFH of the Galaxy. We emphasize that as long as the stars originate from different parts of the disc but still show homogeneous chemical properties, the recovered SFH is representative of the whole population, without the need for specific corrections due to volume effects. While this is less correct for the youngest part of the disc because the stars of this population visible at the solar vicinity explore a restricted range of Galactic radii, it is certainly correct for the thick-disc population.

This method therefore provides a unique and novel way to investigate the history of star formation in the first few Gyr of the formation of the Galaxy, for which there is very little hope of significant progress from counting stars as a function of age, at least before *Gaia* parallaxes become available.

Fitting [Fe/H]-[α/Fe] distributions is a much less effective way to distinguish between models because the chemical tracks are degenerate with time. Without age information it is difficult to constrain the chemical evolution and the SFH. Figure 5 illustrates that the thick-disc [Fe/H]-[α/Fe] data are compatible with SFHs having a broad range of time scales (2−8 Gyr), only a very sharp burst shows a significantly deviating track. Age information is vital to distinguish the SFR from the chemistry alone. Before we summarise our results, a number of limitations and cautionary remarks are worth noting, mainly due to our incomplete knowledge and inconsistency of the stellar yields.

- We required SNII yields from Nomoto et al. (2006) to fit the GCE. The yields from Woosley & Weaver (1995) and Timmes et al. (1995) give a too high final [Si/Fe] ratio.
- We were unable to converge the GCE using the solar abundances of Adibekyan et al. (2012) (Adibekyan et al. 2012 use the iron normalisation from Gonzalez & Laws 2000 that has a value of 7.47). We recovered a track that matched all three projections of the data, but must shift the iron abundance by 0.04 dex (or 10%) to match the age-[Si/Fe] and metallicity-[Si/Fe] plots simultaneously. The recovered SFH changes strikingly if the solar abundance shifts, which changes the relative contributions of the thick and thin disc. Higher solar iron increases the mass of the thick disc, while a low solar iron emphasizes the importance of late-time star formation. However, only solar iron values between 7.49 and 7.53 allowed us to fit the [Fe/H]-[Si/Fe] data for the inner disc.
- We were unable to fit the upper track using magnesium and silicon at the same time. This is because the abundance ratios

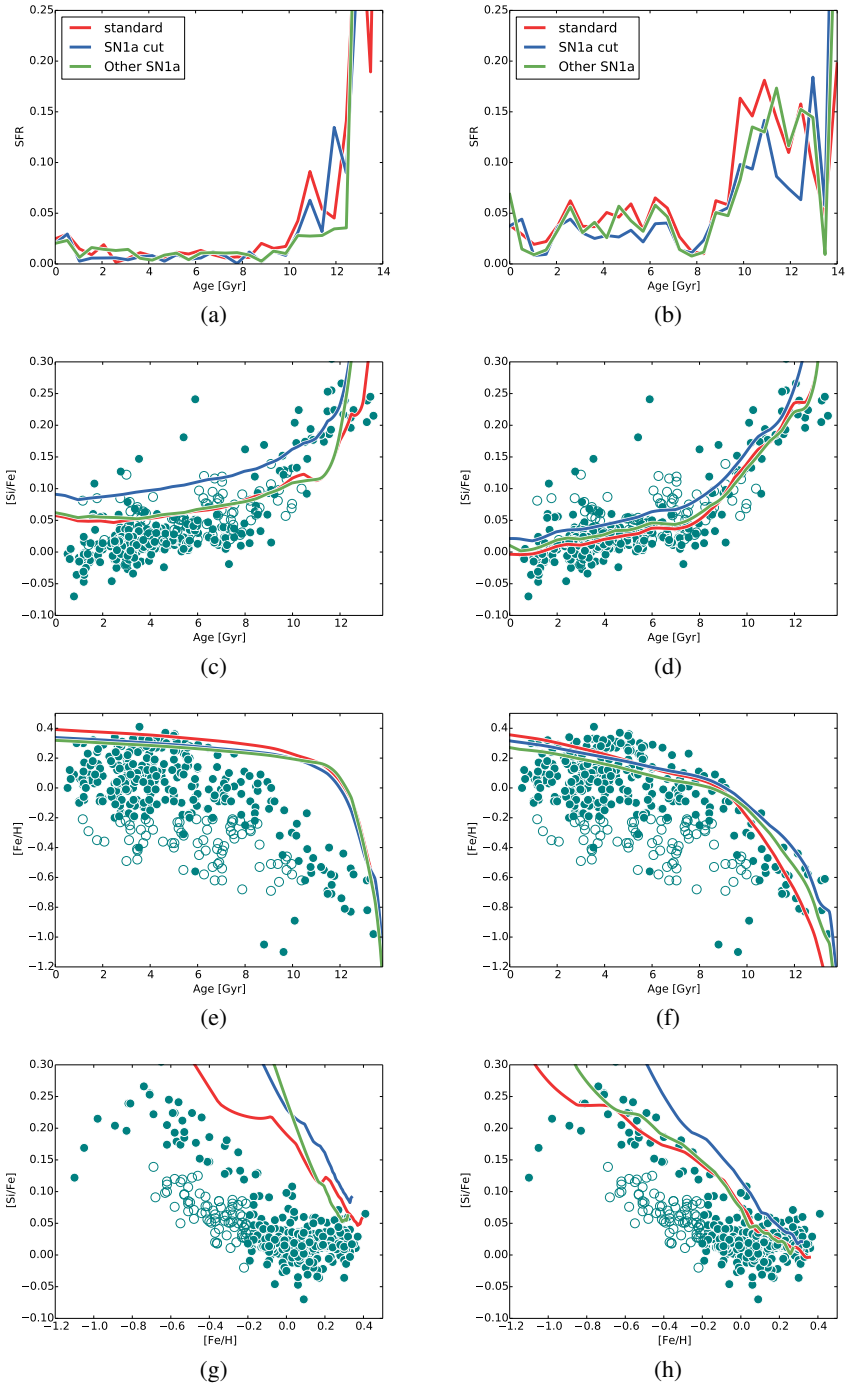

Fig. 18. Comparison of three different models and yields. The left-hand column shows the best-fit chemical tracks for SNII yields from Woosley & Weaver (1995), while the right hand column shows the tracks for SNII yields from Nomoto et al. (2006). The best-fit chemical track and recovered SFH for the standard GCE model summarised in Table 2 is the "standard" track (red line). The blue and green lines are the chemical tracks where a threshold ($Z = 0.1\ Z_{\odot}$) for activating SNIa is included ("the SN1a cut"), and an alternative set of SNIa yields from Travaglio et al. (2004) are used ("Other SN1a"). The recovered SFHs are given in panels **a)** and **b)**, and the standard distributions age-[Si/Fe], age-[Fe/H] and [Fe/H]-[Si/Fe] are given in rows two to four. The points are adapted from Haywood et al. (2013). Open circles are outer thin-disc stars, solid circles are thick-disc and inner thin-disc stars.

between these elements are much lower in the observations than in the model.
- Allowing the normalisation to change (the total fraction of gas used to make stars) introduces some degeneracy into the fitting procedure. However, all normalisations ≥0.5 give similar results within the errors, but we note that lower normalisations produce larger thick-disc components. Normalisations ≤0.5 are too low to fit the age-[Si/Fe] distribution.

With these caveats, our results are as follows:

- Our best-fit SFH for the Milky Way using silicon shows that the Galaxy passed through a phase of intense star formation between ∼9 and 13 Gyr ago.
- This phase was followed by a rapid drop in the SFR (a decrease of 80% in 1 Gyr). For stars of age 9.75 Gyr the SFR has a value of 0.14 Gyr^{-1}, but at 8.75 Gyr it has dropped to 0.06 Gyr^{-1} and by 8.25 Gyr it has fallen to 0.015 Gyr^{-1} at the bottom of the dip (where the integral of the SFH is 1). The SFR apparently stalls for about 1 Gyr. The measured dip was highly robust to all our tests (where $A > 0.8$).
- The SFR recovers after 1 Gyr, at around 7 Gyr, and continues at a lower intensity up to the present.
- The chemical evolution of the outer disc is parallel to that of the thin disc, but starts from different initial conditions: stars of the outer disc start to form ∼2 Gyr before the inner disc, at a higher α-abundance, and at lower metallicity. We require a dilution of metals by three times as much hydrogen to fit

the outer disc distribution, which otherwise shows a flat SFH similar to that of the inner disc.
- Standard IMFs, such as that of Kroupa (2001), allowed us to fit all projections of the chemical tracks at the same time. The Salpeter (1955) IMF gives similar results and the SFH recovered by these two IMFs is very similar within the error.
- The changes to the model discussed in Sect. 6 change the recovered SFH only slightly. The same form is nearly always required, with an early period of vigorous star formation followed by a dip and then a quasi-linear era. However, changes to the canonical model presented in Sect. 5, the yields, or the IMF usually resulted in our being unable to fit the chemical tracks to the data in all three distributions (age-[α/H], age-[Fe/H] or [Fe/H]-[α/Fe]). In general, we either succeeded or failed, without much of a grey area between.

7.2. Interpretation

7.2.1. Life without a (G-dwarf) problem

The results presented above introduce a significant change of perspective regarding chemical evolution modelling of the Milky Way disc. As mentioned in the introduction, most (to our knowledge, all) recent chemical evolution models are based on the need to suppress the formation of too many stars at low metallicity to be in accord with the solar neighbourhood MDF. Several studies in the early 1980s (Chiosi 1980; Lacey & Fall 1985; Matteucci & Greggio 1986; Matteucci & Francois 1989), also motivated by the idea of an inside-out building of discs (Larson 1976), suggested that long-term infall was an elegant solution to this problem. The results presented in the previous section have shown that in apparent contradiction to the solar vicinity, the Galaxy has formed a huge number of dwarfs at intermediate metallicity. While we postpone a detailed discussion of the MDF and the G-dwarf problem to another paper (Haywood et al., in preparation), we briefly comment on this apparent contradiction.

The thick-disc scale length measurement by Bovy et al. (2012) shows that at 1.8 kpc this population has a much shorter scale length than previously thought. Assuming 250 pc, 3.0 kpc, and 90% for the thin-disc scale height, scale length, and local density, and 1000 pc, 10%, and 1.8 kpc for the thick disc, the thin and thick disc would represent 50% of the stellar mass each. This is to be compared with fractions resulting from chemical models assuming infall, wherein the thick disc usually amounts to 15 to 25% at most. Thus, the lack of metal-poor stars is, in this context, a purely local bias[5]. The low-metallicity stars do exist, but they are mostly inside the solar radius. When the Galaxy is taken as a whole, there is no under-abundance of low-metallicity stars. This implies that a near-solar metallicity was attained relatively early in the chemical evolution of the disc, not because of the low dilution permitted by long-term infall, but because the Galaxy formed huge quantities of stars. This permitted the metallicity of the ISM to rise from [Fe/H] < -1.0 dex to about -0.2 dex. Of these stars, a large majority inhabit the inner Galaxy.

The case of the outer disc may be different because it is possible that infall may have contributed on a longer time-scale. Moreover, as already said, the initial metallicity and abundance ratios may have been set by the combination of outflows from the inner disc, and accretion of gas. This means that it is possible that infall models represent the outer disc evolution, although a clear assessment must await new data.

7.2.2. Stellar mass evolution of the Galaxy

The best-fit SFH obtained in Sect. 5.2 (Fig. 7) shows that 52% of the stellar mass formed in the Milky Way disc(s) between 13 and 9 Gyr ago. This percentage confirms the estimate, based on the density parameters given in the previous section, that the thick disc represents half the stellar mass of the disc. The only other component that may have contributed significantly to the general mass growth of the Milky Way at early epochs is the bulge. Most recent results, however, suggest that the contribution from this population is minor. Shen et al. (2010) proposed from adjusting a model to the bulge kinematics data that the Milky Way might be a pure disc galaxy, and that a classical bulge, if present, would not represent more than 10% of the disc stellar mass. This estimate has been confirmed by Kunder et al. (2012). From the Argos survey, Ness et al. (2012) argued that the components they detected in the decomposition of the MDF of the bulge are attributable to the thick and thin discs. Di Matteo et al. (2014) suggested that component B might be due to the young thick disc and confirmed that if a spheroidal component existed in the bulge, it must be small (<10%). These conclusions make the Milky Way fit its local environment: Kormendy et al. (2010) and Fisher & Drory (2012) showed that within 10 and 12 Mpc, the dominant type among giant discs are either pure discs or discs with pseudo-bulges. Hence, we deduce from these studies and from our results that the main component to have formed in the Galaxy at these epochs is the Galactic thick disc. This is in accord with the result by van Dokkum et al. (2013), which shows that progenitors of the Milky Way-type galaxies did not grow a disc starting from a naked bulge.

Moreover, van Dokkum et al. (2013) found that progenitors of the MW have assembled ~50% of their mass at $z \sim 1.5$ (or 9.5 Gyr), well in accord with our findings. Our SFH closely follows the description given by van Dokkum et al. (2013) about MW progenitors: "the implied SFR is approximately constant at 10−15 $M_\odot$ yr^{-1} from $z \sim 2.5$ to $z \sim 1$ then decreases rapidly to ≤ 2 $M_\odot$ yr^{-1} at $z = 0$".

7.3. Comparison with other models

We now discuss our findings in the more general context of chemical evolution models. As already mentioned, analytical chemical evolution models of the Milky Way disc are based on two basic ingredients, the infall of gas on long time-scales (5 Gyr or longer), and a Schmidt-Kennicutt law. The fit to the solar vicinity MDF, a constraint that we discarded, requires that the production of stars of intermediate metallicities is limited, which models achieve through infall, meaning that the metallicity rises in the system by limiting the dilution. We increased the metals in the ISM by allowing a large number of stars of intermediate metallicity to be created. These two radically different views, the one developed here, and the one presented in previous models, makes a direct comparison with previous models somewhat hazardous, particularly since in many studies the thick disc is not considered as a component of the modelling. Although the possible importance of the Galactic thick disc was recognized as early as 1986 (Gilmore & Wyse 1986), this population is rarely explicitly taken into account in models. For instance, there is no explicit thick-disc phase in the models of Fenner & Gibson (2003) or in those of Naab & Ostriker (2006). For infall models

[5] The vertical scale height of the thick disc is considerably longer than the scale height of the thin disc, which further enhances the idea that purely local observations do not sample the average density distribution of low-metallicity stars well. This is discussed in detail in Haywood (2001).

the estimated stellar mass generated before their model reaches a metallicity of −0.2 dex is usually lower than 10% of the total stellar mass.

Chiappini et al. (1997) explicitly considered a halo-thick disc phase with a formation time-scale of 1 Gyr, but its characteristics ([Fe/H] < −1 dex) are difficult to compare with the known properties of the observed thick disc. This follows the low-mass model of the stellar halo of Carney et al. (1990). Fenner & Gibson (2003) used a similar two-phase infall model, based on Chiappini et al. (1997), but considered the first infall phase to be the halo, the thick disc then has thin disc-like properties, and the two are not distinguished. Micali et al. (2013) also explicitly considered a thick-disc phase, where the thick disc is of the order of 25%. Because we did not consider infall, we did not define the history in terms of gas accretion, but in terms of the properties of the SFR. For the infall-based models, the thick-disc phase is relatively short, while the data of Haywood et al. (2013) imply that it lasted approximately 4−6 Gyr, in keeping with our result. Chiappini et al. (1997, 2001) therefore favored a rapidly formed thick disc, while Fenner & Gibson (2003) interpreted their thick disc as a thickened thin disc (Wyse 2001). Both these scenarios are at odds with the interpretation of Haywood et al. (2013), which our model favours. It is important to emphasize that the length of the different phases etc. were not implemented in the model directly, but are the result of using a closed-box model and fitting the data from Haywood et al. (2013). The dip at ages of 8 Gyr (Sect. 5) is superficially reminiscent of the dip at ages of 11 Gyr in the dual-infall model of Chiappini et al. (1997), but it has a different effect. In our model the dip is required, coupled with the large drop in SFR between the inner thin- and thick-disc sequences, to produce a sharp transition at the knee of the age-[Si/Fe] distribution. Chiappini et al. (1997) made the dip serve to allow rapid dilution of [Fe/H], and it allowed the production of the lower sequence in the [Fe/H]-[α/Fe] distribution after the thick disc and halo had formed. Thus, in effect, the thick-disc sequence is constructed separately in the traditional GCE code, with its own infall rate etc, and then the lower sequence is a continuous evolution that occurs subsequently. This does not entirely match the data of Haywood et al. (2013) because the earliest stars in the outer disc sequence are formed concurrently with later stars of the thick disc. In addition, our thick-disc stars continue to be formed until much later than in Chiappini et al. (1997) and its descendants.

To accurately capture the physics of the gas in the Galaxy, a number of different phases of gas need to be considered. The most well-known of these are the low-temperature star-forming gas (HI) in the disc that is capable of forming stars, and the hot gas reservoir that lies in the halo. A third form of gas often invoked to explain the missing baryons is the warm enriched circumgalactic medium, which comprises gas ejected from the disc by feedback (Sommer-Larsen 2006). This accounts for much of the missing mass in a galaxy, that is gas that should be present according to cosmology, but which is not seen in the baryonic mass observed. In traditional closed-box models this warm component is not considered part of the box and is considered an outflow (Hartwick 1976; Matteucci & Chiosi 1983; Prantzos 2003). We did not distinguish between different forms of gas and referred to all different forms of gas in the same manner. As we did not need the HI surface density to control star formation, the gas reservoir was simply a place in which to dilute the metals produced by the stars and that at *some point* forms stars. In effect, our closed box is referred to as such because no gas or metals escape from the system as a whole, but gas and metals are free to change from cold gas to warm gas to hot gas, etc. This is no worse an approximation than any other because the way different modes of gas interact is still largely unknown. Thus, when we say that no gas escapes, we mean, in effect, that it does not escape permanently.

The sensitivity of the chemical evolution to features in the SFH is a dramatic difference. In traditional infall-based models a change of the system can have a very strong effect on the chemical history (Colavitti et al. 2008). The lack of a large reservoir of gas means that metals are not well diluted in the short term. This gas is then cleared out of the system by star formation, and pristine gas falls in. This has two effects on the chemical evolution. It means that the initial increase of metallicity is more rapid (making infall a solution to the G-dwarf problem, as previously discussed), it also has the effect that a burst or hiatus in star formation quickly changes the direction of the chemical track (reducing the chemical inertia). In our case, with a large reservoir of gas, the chemical tracks are slow to change direction because new metals are diluted into an ISM that is massive, and new metals are added to a large quantity of other metals released from previously formed stars. This can be seen by the effect of the dip in the SFR on the [Si/Fe] evolution. Our pause of star formation lowers the [Si/Fe] value by a small amount (Fig. 10). A similar pause in a traditional GCE code has a much more significant effect (Romano et al. 2010; Colavitti et al. 2008).

In traditional GCE models there is apparently little consensus on the "best" parameters. For example, Naab & Ostriker (2006) used a Salpeter IMF, recently Spitoni et al. (2014) or Micali et al. (2013) used a Scalo (1986) IMF, while Fenner & Gibson (2003) used a Kroupa et al. (1993) IMF. The choice of yields remains uncertain (Romano et al. 2010; Kobayashi et al. 2011, etc.). Although we are sensitive to our chosen yields and elements, this is a intrinsic problem of the theoretical yields. Other models similarly provide different results for different elements (e.g. Romano et al. 2010) and yields. There is no clear winner, although some elements and yields fit more poorly than others. For example, Chiappini et al. (1997) used the yields from Woosley & Weaver (1995), while Fenner & Gibson (2003) use results from Limongi et al. (2000) and Limongi & Chieffi (2002) etc. There is no consensus either on the exact functional form linking the gas density to the rate of star formation (Chiosi 1980; Fenner & Gibson 2003; see Matteucci 2009 for a review) or on the exact form infall should take (Colavitti et al. 2008). Another problem with GCE codes is the choice of parameters for which there seems to be little justification, other than just permitting more flexibility to fit the data. For example, Chiappini et al. (1997) changed the star formation efficiencies between the halo/thick-disc phase and the thin-disc phase, while three different star formation efficiencies were adopted in Micali et al. (2013) for the halo, thick-disc and thin-disc phase.

Many GCE codes have attempted to replicate the [Fe/H]-[Si/Fe] distribution alone (e.g. Romano et al. 2010), without any age information. While this is not a difference in the models as such, it is important when classifying the model as one that works well or not. As we showed in Fig. 6, the fitting of SFHs is degenerate without age information. Furthermore, the age-metallicity relation shows considerable scatter, with a spread of almost 1 dex in metallicity at a given age, particularly at more recent times. The age-metallicity relation that is used when any age information is used at all in traditional models (e.g. Chiappini et al. 1997). Thus, we would argue that age information and α-abundances are essential if a GCE model is to be considered a good match to the data.

Our model is much simpler and can fit the data of Haywood et al. (2013) (for silicon) very well. We have interpreted the

model in the context laid out in Haywood et al. (2013), which is somewhat different to that in previous models, and moreover, the parameters of the model were not tuned, except in so far as we required that the chemical tracks actually fit the data to derive a SFH.

8. Conclusions

We have presented a new method of deriving the SFH from stellar abundances, with a full assessment of the possible uncertainties. We derived an SFH for the inner disc ($R < 7$–8 kpc), which shows two distinct phases that correspond to the formation of the thick and the thin discs. The thick-disc formation lasts 4–5 Gyr, during which the SFR reaches 10–15 $M_\odot\,\mathrm{yr}^{-1}$. After the thick-disc phase, star formation stalls for about 1 Gyr and then resumes for the thin-disc phase at a level of 2 $M_\odot\,\mathrm{yr}^{-1}$ for the remaining 7 Gyr. The SFH of the outer disc, as derived from metal-poor thin-disc stars seen at the solar vicinity, shows a similarly flat history, but preceded the thin disc by 2 to 3 Gyr.

The derived SFH implies that the thick disc represents about half the stellar mass formed in the Milky Way, which has been largely unrecognized so far. As discussed in Snaith et al. (2014), the mass growth of the Milky Way seems to be well in accord with the evolution of galaxies of its class.

Overall, our study proposed a change of paradigm in the way we see the first few Gyr of the evolution of the Galactic disc. Up to now, chemical evolution models have described the early building of the Milky Way disc as a slow process. They have been built on the assumption that the thick disc is a minor (in terms of stellar mass) component in order to fit the G-dwarf constraint, but underestimated the role of this population in the chemical evolution of our Galaxy. The closed-box model used here is clearly only a zero-order description of the chemical evolution of the Milky Way. It does not pretend to capture the full complexity of the processes that regulate discs at high redshift, but it is thought to be more suitable than models that use infall on long characteristic time-scales to represent the first few Gyr of the chemical evolution of the Milky Way.

Acknowledgements. The authors acknowledge support from the French Agence Nationale de la Recherche (ANR) under contract ANR-10-BLAN-0508 (Galhis project). Support for ONS was partially provided by NASA through the *Hubble* Space Telescope Archival Research grant HST-AR-12837.01-A from the Space Telescope Science Institute, which is operated by the Association of Universities for Research in Astronomy, Incorporated, under NASA contract NAS5-26555. ONS thanks J. Bailin for interesting discussions that improved the paper. The authors also thank F. Arenou, F. Royer, and C. Babusiaux for their comments. We also thank the anonymous referee for their comments, that improved the quality of the paper.

References

Abadi, M. G., Navarro, J. F., Steinmetz, M., & Eke, V. R. 2003, ApJ, 597, 21
Adibekyan, V. Z., Sousa, S. G., Santos, N. C., et al. 2012, A&A, 545, A32
Allen, C., & Santillan, A. 1991, Rev. Mex. Astron. Astrofis., 22, 255
Anders, E., & Grevesse, N. 1989, Geochim. Cosmochim. Acta, 53, 197
Anders, F., Chiappini, C., Santiago, B. X., et al. 2014, A&A, 564, A115
Asplund, M., Grevesse, N., Sauval, A. J., & Scott, P. 2009, ARA&A, 47, 481
Aumer, M., & White, S. D. M. 2013, MNRAS, 428, 1055
Baldry, I. K., & Glazebrook, K. 2003, ApJ, 593, 258
Bensby, T., Alves-Brito, A., Oey, M. S., Yong, D., & Meléndez, J. 2011, ApJ, 735, L46
Binney, J., & Merrifield, M. 1998, Galactic Astronomy (Princeton University Press)
Bovy, J., Rix, H.-W., Liu, C., et al. 2012, ApJ, 753, 148
Brook, C. B., Stinson, G. S., Gibson, B. K., et al. 2012, MNRAS, 426, 690
Brook, C. B., Stinson, G., Gibson, B. K., et al. 2014, MNRAS, 443, 3809
Brusadin, G., Matteucci, F., & Romano, D. 2013, A&A, 554, A135
Carney, B. W., Latham, D. W., & Laird, J. B. 1990, AJ, 99, 572
Cartledge, S. I. B., Lauroesch, J. T., Meyer, D. M., & Sofia, U. J. 2006, ApJ, 641, 327
Casagrande, L., Ramírez, I., Meléndez, J., Bessell, M., & Asplund, M. 2010, A&A, 512, A54
Chabrier, G. 2003, PASP, 115, 763
Chiappini, C., Matteucci, F., & Gratton, R. 1997, ApJ, 477, 765
Chiappini, C., Matteucci, F., & Romano, D. 2001, ApJ, 554, 1044
Chiosi, C. 1980, A&A, 83, 206
Colavitti, E., Matteucci, F., & Murante, G. 2008, A&A, 483, 401
Demarque, P., Woo, J.-H., Kim, Y.-C., & Yi, S. K. 2004, ApJS, 155, 667
Di Matteo, P., Haywood, M., Gómez, A., et al. 2014, A&A, 567, A122
Diehl, R., Halloin, H., Kretschmer, K., et al. 2006, Nature, 439, 45
Fenner, Y., & Gibson, B. K. 2003, PASA, 20, 189
Fenner, Y., Gibson, B. K., & Limongi, M. 2002, Astrophys. Space Sci., 281, 537
Few, C. G., Courty, S., Gibson, B. K., et al. 2012, MNRAS, 424, L11
Fisher, D. B., & Drory, N. 2012, in Am. Astron. Soc. Meet. Abstr., 219, 417.01
François, P., Matteucci, F., Cayrel, R., et al. 2004, A&A, 421, 613
Fuhrmann, K., Chini, R., Hoffmeister, V. H., & Bernkopf, J. 2012, MNRAS, 420, 1423
Gibson, B. K., Pilkington, K., Brook, C. B., Stinson, G. S., & Bailin, J. 2013, A&A, 554, A47
Gilmore, G., & Wyse, R. F. G. 1986, Nature, 322, 806
Gonzalez, G., & Laws, C. 2000, AJ, 119, 390
Greggio, L. 2005, A&A, 441, 1055
Hartwick, F. D. A. 1976, ApJ, 209, 418
Haywood, M. 2001, MNRAS, 325, 1365
Haywood, M. 2006, MNRAS, 371, 1760
Haywood, M. 2008, MNRAS, 388, 1175
Haywood, M. 2014, Mem. Soc. Astron. It., 85, 253
Haywood, M., Di Matteo, P., Lehnert, M. D., Katz, D., & Gómez, A. 2013, A&A, 560, A109
Hopkins, A. M., & Beacom, J. F. 2006, ApJ, 651, 142
Iwamoto, K., Brachwitz, F., Nomoto, K., et al. 1999, ApJS, 125, 439
Jørgensen, B. R., & Lindegren, L. 2005, A&A, 436, 127
Jurić, M., Ivezić, Ž., Brooks, A., et al. 2008, ApJ, 673, 864
Karakas, A. I. 2010, MNRAS, 403, 1413
Kawata, D., & Gibson, B. K. 2003, MNRAS, 340, 908
Kennicutt, Jr., R. C. 1983, ApJ, 272, 54
Kennicutt, Jr., R. C. 1998, ApJ, 498, 541
Kobayashi, C., Tsujimoto, T., Nomoto, K., Hachisu, I., & Kato, M. 1998, ApJ, 503, L155
Kobayashi, C., Tsujimoto, T., & Nomoto, K. 2000, ApJ, 539, 26
Kobayashi, C., Karakas, A. I., & Umeda, H. 2011, MNRAS, 414, 3231
Kordopatis, G., Gilmore, G., Wyse, R. F. G., et al. 2013, MNRAS, 436, 3231
Kormendy, J., Drory, N., Bender, R., & Cornell, M. E. 2010, ApJ, 723, 54
Kroupa, P. 2001, MNRAS, 322, 231
Kroupa, P., Tout, C. A., & Gilmore, G. 1993, MNRAS, 262, 545
Kunder, A., Koch, A., Rich, R. M., et al. 2012, AJ, 143, 57
Lacey, C. G., & Fall, S. M. 1985, ApJ, 290, 154
Larson, R. B. 1976, MNRAS, 176, 31
Lilly, S. J., Le Fevre, O., Hammer, F., & Crampton, D. 1996, ApJ, 460, L1
Limongi, M., & Chieffi, A. 2002, PASA, 19, 246
Limongi, M., Straniero, O., & Chieffi, A. 2000, ApJS, 129, 625
Madau, P., & Dickinson, M. 2014, ARA&A, 52, 415
Madau, P., Ferguson, H. C., Dickinson, M. E., et al. 1996, MNRAS, 283, 1388
Madau, P., Pozzetti, L., & Dickinson, M. 1998, ApJ, 498, 106
Mannucci, F., Della Valle, M., Panagia, N., et al. 2005, A&A, 433, 807
Mannucci, F., Della Valle, M., & Panagia, N. 2006, MNRAS, 370, 773
Matteucci, F. 2009, in Chemical evolution, ed. J. Cepa (Cambridge University Press), 183
Matteucci, F., & Chiosi, C. 1983, A&A, 123, 121
Matteucci, F., & Francois, P. 1989, MNRAS, 239, 885
Matteucci, F., & Greggio, L. 1986, A&A, 154, 279
Matteucci, F., Spitoni, E., Recchi, S., & Valiante, R. 2009, A&A, 501, 531
McMillan, P. J. 2011, MNRAS, 414, 2446
Micali, A., Matteucci, F., & Romano, D. 2013, MNRAS, 436, 1648
Morrison, H. L., Flynn, C., & Freeman, K. C. 1990, AJ, 100, 1191
Naab, T., & Ostriker, J. P. 2006, MNRAS, 366, 899
Nelder, J. A., & Mead, R. 1965, Comput. J., 7, 308

Ness, M., Freeman, K., Athanassoula, E., et al. 2012, ApJ, 756, 22
Nidever, D. L., Bovy, J., Bird, J. C., et al. 2014, ApJ, 796, 38
Nittler, L. R. 2005, ApJ, 618, 281
Nomoto, K., Tominaga, N., Umeda, H., Kobayashi, C., & Maeda, K. 2006, Nucl. Phys. A, 777, 424
Pagel, B. E. J., & Patchett, B. E. 1975, MNRAS, 172, 13
Pagel, B. E. J., & Tautvaisiene, G. 1997, MNRAS, 288, 108
Powell, M. J. D. 1964, Comput. J., 7, 155
Prantzos, N. 2003, A&A, 404, 211
Raiteri, C. M., Villata, M., & Navarro, J. F. 1996, A&A, 315, 105
Ramírez, I., Allende Prieto, C., & Lambert, D. L. 2013, ApJ, 764, 78
Reddy, B. E., Lambert, D. L., & Allende Prieto, C. 2006, MNRAS, 367, 1329
Robitaille, T. P., & Whitney, B. A. 2010, ApJ, 710, L11
Romano, D., Chiappini, C., Matteucci, F., & Tosi, M. 2005, A&A, 430, 491
Romano, D., Karakas, A. I., Tosi, M., & Matteucci, F. 2010, A&A, 522, A32
Salpeter, E. E. 1955, ApJ, 121, 161
Scalo, J. M. 1986, Fundamental Cosmic Physics, 11, 1
Scalo, J. 1998, in The Stellar Initial Mass Function (38th Herstmonceux Conf.), eds. G. Gilmore, & D. Howell, ASP Conf. Ser., 142, 201
Schmidt, M. 1959, ApJ, 129, 243
Schmidt, M. 1963, ApJ, 137, 758
Shen, J., Rich, R. M., Kormendy, J., et al. 2010, ApJ, 720, L72
Snaith, O. N., Haywood, M., Di Matteo, P., et al. 2014, ApJ, 781, L31
Sommer-Larsen, J. 2006, ApJ, 644, L1
Spitoni, E., Matteucci, F., & Sozzetti, A. 2014, MNRAS, 440, 2588
Stinson, G. S., Brook, C., Macciò, A. V., et al. 2013, MNRAS, 428, 129
Tacconi, L. J., Genzel, R., Neri, R., et al. 2010, Nature, 463, 781
Timmes, F. X., Woosley, S. E., & Weaver, T. A. 1995, ApJS, 98, 617
Tinsley, B. M. 1974, ApJ, 192, 629
Travaglio, C., Hillebrandt, W., Reinecke, M., & Thielemann, F.-K. 2004, A&A, 425, 1029
van den Bergh, S. 1962, AJ, 67, 486
van Dokkum, P. G., Leja, J., Nelson, E. J., et al. 2013, ApJ, 771, L35
Woosley, S. E., & Weaver, T. A. 1995, ApJS, 101, 181
Wyse, R. F. G. 2001, in Galaxy Discs and Disc Galaxies, eds. J. G. Funes, & E. M. Corsini, ASP Conf. Ser., 230, 71
Yamada, S., Suda, T., Komiya, Y., Aoki, W., & Fujimoto, M. Y. 2013, MNRAS, 436, 1362